Selective CDK9 inhibition resolves neutrophilic inflammation and enhances cardiac regeneration in larval zebrafish

Selective CDK9 inhibition resolves neutrophilic inflammation and enhances cardiac regeneration in larval zebrafish

[1]Aryan Kaveh, [1]Finnius A Bruton, [2]Magdalena EM Oremek, [1]Carl S Tucker, [3]Jonathan M Taylor, [1]John J Mullins, [2]Adriano G Rossi, [1]Martin A Denvir

[1]Centre for Cardiovascular Science, Queen's Medical Research Institute, University of Edinburgh, Edinburgh, United Kingdom

[2]Centre for Inflammation Research, Queen's Medical Research Institute, University of Edinburgh, Edinburgh, United Kingdom

[3]Department of Physics, University of Glasgow, Glasgow, United Kingdom

Corresponding author: Aryan Kaveh (Aryan.Kaveh@ed.ac.uk)

Key words: cardiac, regeneration, zebrafish, AT7519, neutrophil, resolution

Summary Statement

This study is the first to show that resolving neutrophilic inflammation using a clinically approved immunomodulatory drug (AT7519) improves heart regeneration in zebrafish.

Abstract

Sustained neutrophilic inflammation is detrimental for cardiac repair and associated with adverse outcomes following myocardial infarction (MI). An attractive therapeutic strategy to treat MI is to reduce or remove infiltrating neutrophils to promote downstream reparative mechanisms. CDK9 inhibitor compounds enhance the resolution of neutrophilic inflammation, however, their effects on cardiac repair/regeneration are unknown. Our laboratory has devised a cardiac injury model to investigate inflammatory and regenerative responses in larval zebrafish using heartbeat-synchronised light sheet fluorescence microscopy. We used this model to test two clinically approved CDK9 inhibitors, AT7519 and Flavopiridol, examining their effects on neutrophils, macrophages and cardiomyocyte regeneration. We found AT7519 and Flavopiridol resolve neutrophil infiltration by inducing reverse migration from the cardiac lesion. While continuous exposure to AT7519 or Flavopiridol caused adverse phenotypes, transient treatment accelerated neutrophil resolution while avoiding these effects. Transient treatment with AT7519, but not Flavopiridol, augmented wound-associated macrophage polarisation, which enhanced macrophage-dependent cardiomyocyte number expansion and the rate of myocardial wound closure. Using *cdk9*$^{-/-}$ knockout mutants we showed AT7519 is a selective CDK9 inhibitor, revealing the potential of such treatments to promote cardiac repair/regeneration.

Introduction

Myocardial infarction (MI) is a leading cause of morbidity and mortality worldwide. MI occurs when a coronary artery occludes, leading to myocardial ischaemia and extensive cardiomyocyte death. The surviving myocardium subsequently undergoes compensatory remodelling and scarring, which often results in secondary complications such as heart failure. Although MI can be successfully treated and managed (Anderson and Morrow, 2017), there are no approved therapies that promote repair of the damaged myocardium. Recent clinical trials have investigated immunomodulatory therapies that inhibit pleiotropic inflammatory pathways (Ridker et al., 2017 and Tardif et al., 2019). These treatments lower the incidence of cardiovascular events post-MI but increase the risk of infections. Therefore, there is a need to explore treatments that specifically target myocardial inflammation and promote downstream cardiac repair mechanisms following MI.

Neutrophils are the first immune cell recruited to the myocardial infarct where they phagocytose dead and dying cells (Dewald et al., 2004 and Swirski and Nahrendorf, 2013). Neutrophils subsequently secrete inflammatory mediators to recruit monocytes, which later differentiate into macrophages (Dewald et al., 2005 and Nahrendorf et al., 2007). Once the acute inflammatory response starts to resolve, most infiltrating neutrophils undergo apoptosis (Daseke et al., 2019). Apoptotic neutrophils are efferocytosed by inflammatory macrophages, triggering a series of anti-inflammatory pathways that promote cardiac repair (Savill et al., 2002; Schwab et al., 2007; Frangogiannis, 2012 and Ma et al., 2013). Conversely, defective clearance of neutrophils augments inflammation, promoting cardiomyocyte apoptosis, infarct expansion and adverse structural remodelling (Frangogiannis et al., 2002; Vinten-Johansen, 2004; Garlichs et al., 2004; van Hout et al., 2015 and Schloss et al., 2016). Indeed, blood neutrophilia is recognised as an indicator of adverse clinical outcomes following MI (Arruda-Olson et al., 2009 and Chia et al., 2009). Resolving cardiac-recruited neutrophils therefore has potential as a viable therapeutic strategy to improve myocardial repair post-MI.

Extensive work from our group and others has shown that cyclin-dependent kinase 9 (CDK9) inhibitor compounds selectively induce neutrophil apoptosis, reduce neutrophil infiltration, and promote the resolution of inflammation *in vitro* and *in vivo* (Rossi et al., 2006; Loynes et al., 2010; Leitch et al., 2012; Wang et al., 2012; Lucas et al., 2014; and Hoodless et al., 2016). Unlike most other CDKs, CDK9 specifically regulates the transcription of primary inflammatory response genes via RNA Polymerase II. These include inflammatory cytokines and the neutrophil pro-survival protein, Mcl-1 (Sundar et al., 2020; Eyvazi et al.,

2019 and Lucas et al., 2014). Acute inhibition of CDK9 therefore provides a therapeutic opportunity to preferentially suppress the transcription of short-lived inflammatory disease drivers. However, due to the conserved structure of CDKs, CDK9 inhibitor compounds may also target other kinases (Krystof et al., 2012). Two potent CDK9 inhibitors, AT7519 and Flavopiridol (FVP), have been widely used in clinical trials as anti-cancer therapies (Mahadevan et al., 2011; Chen et al., 2014; Luke et al., 2012 and Awan et al., 2016). Our group has shown that AT7519 and FVP drive neutrophil apoptosis in a CDK9-dependent manner to resolve inflammation following tail fin transection in larval zebrafish (Hoodless et al., 2016). It is not yet understood how CDK9 inhibitors influence inflammatory and repair/regeneration responses following tissue wounding.

The zebrafish has proven to be an essential model for studying cardiac injury, repair and regeneration. Unlike adult mammalian hearts, zebrafish hearts regenerate rapidly following injury via cardiomyocyte proliferation (Poss et al., 2002; Jopling et al., 2010 and Kikuchi et al., 2010). Adult zebrafish cardiac injury and regeneration studies have found that sustained neutrophil retention inhibits cardiomyocyte proliferation, promotes cardiomyocyte apoptosis and delays scar regression (Lai et al., 2017 and Xu et al., 2019). The resolution of neutrophilic inflammation is therefore considered a prerequisite for timely and complete heart regeneration. We recently characterised neutrophil and macrophage migratory responses in larval zebrafish cardiac injury using bespoke live imaging (Taylor et al., 2019 and Kaveh et al., 2020). We found a conserved sequence of events marked by an early and acute phase of neutrophil recruitment followed by sustained macrophage recruitment (Kaveh et al., 2020). Importantly, the dynamics of the immune cell response in larval zebrafish closely recapitulates that of adult zebrafish and murine models of cardiac injury (Bevan et al., 2020 and Epelman et al., 2015).

In this study, we use our established larval zebrafish cardiac injury model to investigate whether CDK9 inhibitor (CDK9i) treatment with AT7519 or FVP resolves neutrophil infiltration and examine whether this regulates downstream macrophage involvement and cardiac regeneration. We found both AT7519 and FVP resolved neutrophilic inflammation via reverse migration. However subsequent drug exposure caused adverse effects, which were avoided by shortening treatment duration. Interestingly, transient (pulsed) treatment with AT7519, but not FVP, enhanced *tnf* expression in wound-associated macrophages, in turn promoting macrophage-dependent cardiomyocyte number expansion and the rate of myocardial wound closure. We show that unlike FVP, AT7519 is a selective CDK9 inhibitor and thus a promising immunomodulatory treatment that can promote cardiomyocyte regeneration.

114

Results

CDK9i treatment resolves neutrophil infiltration by promoting reverse migration from the cardiac injury site

We have previously characterised cardiac injury, neutrophil recruitment and resolution dynamics following ventricular laser injury in larval zebrafish. We found peak neutrophil infiltration occurs at 6 hours post injury (hpi) and neutrophil numbers entirely resolve by 48 hpi (Kaveh et al., 2020). Two CDK9 inhibitors, AT7519 and Flavopiridol (FVP), have been shown to resolve wound-recruited neutrophil numbers by inducing apoptosis following larval zebrafish tail fin transection (Hoodless et al., 2016). To avoid disrupting the onset of inflammation in our cardiac injury model, and encourage the resolution of peak neutrophilic inflammation, *Tg(myl7:GFP;mpx:mCherry)* larvae were treated continuously with AT7519 or FVP from 4hpi. Larvae were subsequently imaged at 6 hpi and 24 hpi using epifluorescence microscopy to quantify ventricular neutrophil numbers (Figure 1A). Following recruitment to the injured ventricular apex at 4 hpi, neutrophil numbers increased in DMSO vehicle-treated larvae at 6 hpi (Figure 1B and 1C). In contrast, fewer ventricular neutrophils were present in larvae treated with 50μM AT7519 or 3μM FVP at 6 hpi (1.8 ± 0.3 vs 3.6 ± 0.5 and 1.8 ± 0.4 vs 3.7 ± 0.6) (Figure 1B and 1C). Neutrophil presence decreased in all groups at 24 hpi, indicating neutrophil numbers had mostly resolved (Figure 1B and 1C). To determine whether this drug-induced reduction in cardiac-neutrophil numbers was due to cell death or reverse migration, timelapse images were acquired using heartbeat-synchronised light sheet fluorescence microscopy (LSFM) (Taylor et al., 2019). Live imaging demonstrated that recruited neutrophils cluster specifically at the cardiac injury site in DMSO vehicle-treated larvae (Supplementary Video 1), as previously shown (Kaveh et al., 2020). This is displayed in Figure 1D where neutrophil positions are temporally colour coded between 4 hpi and 6 hpi, allowing neutrophil migration to be schematically summarised. Following treatment with AT7519 (Supplementary Video 2) or FVP (Supplementary Video 3), recruited neutrophils appeared to migrate more erratically and subsequently reverse migrated to the pericardium anteriorly or posteriorly from the ventricle by 6 hpi (Figure 1D and 1F). These data demonstrate that CDK9i drug treatment accelerates the resolution of peak neutrophilic inflammation at the cardiac injury site dynamically by reverse migration. As our timelapse imaging can account for every wound-recruited immune cell (Kaveh et al., 2020), these findings exclude neutrophil apoptosis or the efferocytosis of apoptotic neutrophils as a resolution mechanism with CDK9i treatment in this model.

Continuous CDK9i treatment reduces macrophage retention by promoting reverse migration from the injured heart

Having established CDK9i treatment induces neutrophil reverse migration following cardiac injury, macrophage involvement was next examined. We have previously described macrophage recruitment dynamics in this model. Unlike the neutrophil response, macrophage recruitment occurs up to 24 hpi, with their numbers decreasing but not returning to baseline by 48 hpi (Kaveh et al., 2020). To test the effect of CDK9i treatment during the macrophage response to cardiac injury, *Tg(myl7:GFP;mpeg1:mCherry)* larvae were treated continuously with AT7519 or FVP from 4 hpi and subsequently imaged at 6 hpi, 24 hpi and 48 hpi (Figure 2A). In the presence of AT7519 or FVP, ventricular macrophage numbers were unaffected until 24 hpi, at which point significantly fewer macrophages were present with AT7519 (8.3 ± 0.6 vs 10.9 ± 0.7) or FVP (3.7 ± 0.7 vs 10.6 ± 0.9) (Figure 2B). This attenuated macrophage presence was more pronounced with FVP, where macrophage numbers were as low as uninjured larvae (Figure 2B). At 48 hpi, ventricular macrophage numbers remained diminished with FVP treatment (3.7 ± 0.6 vs 8.7 ± 0.9), similarly AT7519-treated larvae displayed a further decrease in recruited macrophage numbers (4.9 ± 0.6 vs 8.0 ± 0.8) (Figure 2B). LSFM timelapse imaging indicated that cardiac-recruited macrophages gradually undergo reverse migration in the presence of FVP, as opposed to being retained on the injured ventricle in control conditions (Supplementary Video 4, Supplementary Video 5 and Figure 2C).

Continuous CDK9i treatment disrupts cardiac function and cardiomyocyte number expansion

While examining the macrophage response with CDK9i treatment, it became apparent that ventricular contractility was being compromised at the later timepoints. Ventricular ejection fraction was diminished with FVP at 24 hpi and 48 hpi, and with AT7519 at 48 hpi, in both uninjured and cardiac-injured larvae (Figure 2–supplement 1B). Contrastingly, DMSO vehicle-treated cardiac-injured larvae displayed a complete functional recovery of ejection fraction by 48 hpi (Figure 2–supplement 1B). Similar to ejection fraction, heart rate was also significantly reduced with FVP at 48 hpi in uninjured and injured larvae (Figure 2–supplement 1C). To identify if this loss in cardiac function is associated with a change in cardiomyocyte numbers, ventricular cardiomyocyte nuclei were quantified using *Tg(myl7:DsRed2-NLS)* larvae and LSFM. No differences were observed between groups at 24 hours post treatment (hpt). At 48 hpt, however, fewer ventricular cardiomyocytes were observed in the presence of AT7519 (251.6 ± 17.5 vs 272.7 ± 14.9) and FVP (241.7 ± 21.6 vs 269.3 ± 17.3) compared to DMSO vehicle (Figure 2D and 2E). These data indicate that continuous CDK9i treatment suppresses cardiac function and the expansion of cardiomyocyte numbers.

Continuous CDK9i treatment does not affect global macrophage numbers but causes neutropenia

Having identified undesirable cardiac-specific effects with continuous CDK9i treatment, we tested if these compounds altered whole-body macrophage or neutrophil numbers by serially imaging *Tg(mpeg1:mCherry)* or *Tg(mpx:mCherry)* larvae. Across all experimental timepoints and treatment groups, whole-body macrophage numbers were unaffected and increased steadily, as expected with normal development (Figure 2–supplement 2A). However, at 48 hpi, significantly fewer neutrophils were present globally with AT7519 (253.7 ± 17.7 vs 318.1 ± 18.8) and FVP (218.8 ± 15.9 vs 280.9 ± 8.7) compared to their DMSO vehicle-treated counterparts (Figure 2–supplement 2B and 2C). Closer examination of CDK9i-treated neutropenic larvae showed that some neutrophils appear condensed and rounded – two properties of an apoptotic cell (Figure 2–supplement 2D). Thus, these data suggest that continuous exposure to CDK9 inhibitors promotes neutrophil but not macrophage cell death, corroborating previous studies (Lucas et al., 2014 and Hoodless et al., 2016).

Transient CDK9i treatment resolves neutrophilic inflammation without causing neutropenia or impairing cardiac contractility

To avoid adverse cardiac effects and neutropenia apparent at the later timepoints with CDK9i treatment, the duration of treatment was modified. We previously showed that peak neutrophilic inflammation at 6 hpi resolves by treating larvae with AT7519 or FVP from 4 hpi (Figure 1). Therefore, a shorter treatment was adopted where larvae were specifically treated with AT7519 or FVP for two hours from 4 hpi (Figure 3–supplement 1A). We first confirmed that cardiac-recruited neutrophil numbers were reduced following transient (pulsed) CDK9i treatment (Figure 3–supplement 1B). Unlike continuous CDK9i treatment, the transient treatment was not associated with neutropenia (Figure 3–supplement 1C). We next assessed ventricular ejection fraction as this was noticeably diminished during continuous CDK9i treatments (Figure 2–supplement 1B). Following transient CDK9i treatment with AT7519 or FVP ejection fraction recovered promptly, with injured treatment groups displaying no differences across all timepoints (Figure 3–supplement 1D).

Transient CDK9i treatment retains cardiac macrophage numbers following injury and AT7519 enhances wound macrophage *tnf* expression

As macrophages are essential for complete myocardial repair (Ma et al., 2018), we next tested whether the revised transient CDK9i treatment (Figure 3A) alters ventricular macrophage wound accumulation and/or polarisation. In contrast to mammalian models, only one macrophage polarisation marker has been reliably reported in larval zebrafish and this is TNF. These studies revealed *tnf*$^{+}$ macrophages to have pro-regenerative properties

following spinal cord, somitic muscle and tail fin injury (Cavone et al., 2021; Tsarouchas et al., 2018; Gurevich et al., 2018 and Nguyen-Chi et al., 2017). As such, the hearts of *Tg(mpeg1:mCherry;TNFa:GFP)* larvae were analysed using LSFM following cardiac injury. Unlike continuous CDK9i treatment, ventricular macrophage retention was unaffected following transient treatment with AT7519 or FVP (Figure 3B, 3C and 3E). Furthermore, following transient AT7519 treatment, a significant increase in ventricular *tnf*$^{+}$ macrophages was observed at 24 hpi compared to their DMSO vehicle-treated counterparts (8.8 ± 4.8 vs 4.0 ± 3.7), which returned to baseline at 48 hpi (5.0 ± 4.1 vs 4.0 ± 3.4) (Figure 3B and 3D). Interestingly, this effect was not detected following transient FVP treatment, as no statistical difference was found in ventricular *tnf*$^{+}$ macrophage numbers at 24 hpi (5.2 ± 5.3 vs 3.2 ± 3.2) (Figure 3B and 3E). The increase in *tnf*$^{+}$ cardiac macrophages following transient AT7519 treatment was not observed when applied to uninjured larvae (Figure 3–supplement 2), suggesting this effect to be injury-specific. LSFM timelapse imaging demonstrated that *tnf*$^{+}$ macrophages can migrate from the pericardium onto the injured ventricle, or, what appears to be more common is that wound-proximal macrophages upregulate *tnf* (Supplementary Video 6 and Figure 3F). Together these data indicate that transient CDK9i treatment does not affect cardiac macrophage wound accumulation, and AT7519 enhances *tnf* expression in wound-associated macrophages.

AT7519 is a more selective CDK9 inhibitor than Flavopiridol in zebrafish

To better understand the differential phenotypes observed with AT7519 and FVP treatment, we next explored the selectivity of these two CDK9 inhibitor compounds in larval zebrafish. Drug screening studies *in vitro* have suggested that AT7519 is a more selective CDK9 inhibitor compared to first-generation CDK9 inhibitors such as FVP (Santo et al., 2010 and Liu et al., 2011). We formally tested the Cdk9 selectivity of these inhibitors *in vivo* using stable *cdk9* knockout zebrafish generated using CRISPR/Cas9 (Hoodless et al., 2016). Homozygous *cdk9* mutant zebrafish larvae are phenotypically distinguishable at 3 days post fertilisation (dpf) (Hoodless et al., 2016). Compared to their heterozygous and wild-type siblings, homozygous *cdk9* mutants display a curved body axis, shorter body length and smaller eye diameter (Figure 4A). No phenotypic differences were identified between heterozygous mutants and wild-type siblings up to 5 dpf (Figure 4A), which was confirmed by genotyping (Figure 4B). We reasoned that a truly selective CDK9 inhibitor would not have any effect on *cdk9*$^{-/-}$ knockout zebrafish larvae. To test this, we continuously treated 3 dpf homozygous *cdk9* mutants with DMSO vehicle, AT7519 or FVP and quantified heart rate between treatments as a readout for overall health across 48 hours. We have shown that continuous CDK9i treatment causes wild-type larvae to develop bradycardia (Figure 2–supplement 1C) and heart rate is a recognised readout of drug-induced toxicity in larval

zebrafish (Rubinstein, 2006 and Kithcart and MacRae, 2017). Thus, a decline in heart rate with AT7519 or FVP compared to vehicle would suggest the compounds are acting in a Cdk9-independent manner. First, larvae were treated at 1μM concentrations of AT7519 or FVP (or DMSO vehicle) so that CDK9i treatments were fair and comparable. Between 2 hpt and 48 hpt, all treatment groups displayed a gradual reduction in heart rate, which was associated with decreased survival from 24 hpt (Figure 4C and 4E). At 24 hpt, compared to the DMSO vehicle group, FVP-treated, but not AT7519-treated, mutant larvae displayed a significant reduction in heart rate (22.5 ± 8.9 vs 80.4 ± 6.6 and 63.2 ± 8.6 vs 80.4 ± 6.6), which was associated with increased mortality (64.3% vs 14.3%) (Figure 4C and 4E). The heart rates of larvae treated with AT7519 were unchanged across all timepoints and displayed a more gradual reduction, similar to their DMSO vehicle-treated counterparts (Figure 4C and 4E). To draw direct comparisons between drug selectivity and the differential phenotypes observed, we applied the drug concentrations established originally for resolving neutrophilic inflammation (50μM for AT7519 and 3μM for FVP). Using these concentrations, FVP-treated mutant larvae displayed significantly lowered heart rates from 2 hpt (90.0 ± 6.7 vs 117.1 ± 6.2) until 12 hpt (64.3 ± 6.5 vs 99.6 ± 4.9) compared to their DMSO vehicle-treated and AT7519-treated counterparts, which showed no differences across these timepoints (Figure 4D). Until 12 hpt, this FVP-induced reduction in heart rate was not associated with a change in survival (Figure 4F). At 24 hours post FVP treatment, 14% of larvae survived, all of which displayed diminished heart rates (Figure 4D and 4F). In contrast, at 24 hours post AT7519 treatment survival only decreased to 93%, but the heart rates of these larvae were lower compared to their DMSO vehicle-treated counterparts (60.0 ± 9.0 vs 88.2 ± 8.7) (Figure 4D and 4F). At 48 hpt, no larvae survived with FVP and AT7519, whereas 36% of DMSO vehicle-treated survived (Figure 4D and 4F). In summary, we have developed a proof-of-concept assay using knockout larval zebrafish mutants to examine drug selectivity *in vivo*. The assay indicated whether AT7519 and FVP exhibit Cdk9-independent effects up to 48 hpt, with FVP displaying significant off-target effects from 2 hpt. These comparative zebrafish data suggest that AT7519 is a particularly selective CDK9 inhibitor *in vivo*.

Transient AT7519 but not Flavopiridol treatment enhances cardiomyocyte number expansion following injury

We next tested whether the differing regulation of macrophage *tnf* polarisation following transient CDK9i treatment (Figure 3) influenced cardiomyocyte numbers. Following transient AT7519 or FVP treatment (Figure 5A), LSFM scans of *Tg(myl7:DsRed2-NLS)* larvae indicated no change in ventricular cardiomyocyte numbers at 24 hpi (Figure 5C). At 48 hpi, however, ventricular cardiomyocyte numbers were significantly elevated following AT7519

treatment (321.6 ± 31.7 vs 292.7 ± 23.5) (Figure 5B and 5C), indicating an increase in cardiomyocyte number expansion. At 48 hpi following FVP treatment no difference in cardiomyocyte numbers was present (298.0 ± 22.5 vs 298.8 ± 25.8) (Figure 5B and 5C). This AT7519-specific increase in cardiomyocyte numbers was injury-specific as uninjured larvae displayed no change in ventricular cardiomyocyte numbers following the same treatment (Figure 5–supplement 1).

Transient AT7519 treatment accelerates structural myocardial regeneration following injury

We have previously shown that laser injury induces cardiomyocyte death locally at the ventricular apex (Kaveh et al., 2020). In order to determine whether the increase in cardiomyocyte numbers identified with transient AT7519 treatment is associated with improved structural myocardial regeneration, LSFM scans of cardiac-injured *Tg(myl7:GFP)* larvae were acquired and the ventricular wound area was quantified (Figure 5D). At 24 hpi myocardial wound area was similar between DMSO vehicle-treated and AT7519-treated groups (109.2 ± 84.8μm^2 vs 100.9 ± 59.3μm^2) (Figure 5E and 5F). At 48 hpi, both groups displayed a reduction in wound area, although the DMSO vehicle group trended towards a larger wound area compared to the AT7519 group (53.1 ± 57.6μm^2 vs 29.9 ± 30.2μm^2) (Figure 5E and 5F). To better understand the rate of wound regression in these groups, percentage myocardial wound closure between 24 hpi and 48 hpi was analysed. This indicated a clear increase in wound closure following AT7519 treatment compared to controls (69.6% vs 21.2%) (Figure 5G), highlighting an acceleration in the rate of myocardial wound regression. To closely examine how the myocardial wound structurally regenerates, LSFM timelapse images were acquired. Live heartbeat-synchronised timelapse imaging revealed that wound-proximal cardiomyocytes protrude into, and subsequently bridge across, the injured myocardium to regenerate the damaged tissue (Supplementary Video 7 and Figure 5E and 5H).

Macrophages are required for the improved cardiomyocyte regenerative response following AT7519 treatment

To determine whether macrophages are involved in the AT7519-associated increase in cardiomyocyte numbers following injury, we generated macrophage-null (*irf8* homozygous mutant) transgenic zebrafish to analyse cardiomyocyte nuclei numbers using LSFM. First, we incrossed heterozygous *irf8* mutants on a *Tg(myl7:h2b-GFP)* background and genotyped the offspring, selecting a population of wild-type and homozygous *irf8* mutants (Figure 6A). Neutral red staining clearly demonstrated that *irf8*$^{+/+}$ larvae were marked with macrophages/microglia in the brain, whereas their *irf8*$^{-/-}$ counterparts completely lacked such

staining (Shiau et al., 2015) and thus macrophages/microglia (Figure 6B). Next, we cardiac injured macrophage-replete (*irf8*$^{+/+}$) and macrophage-null (*irf8*$^{-/-}$) larvae and subsequently administered the transient AT7519 treatment. Analysis of macrophage-replete (*irf8*$^{+/+}$) larvae at 48 hpi showed an increase in cardiomyocyte numbers with AT7519 compared to DMSO vehicle, as established previously (Figure 6C, 6D and Figure 5C). Macrophage-null (*irf8*$^{-/-}$) larvae, however, did not display an injury-associated increase in cardiomyocyte numbers (Figure 6C and 6D), suggesting that macrophages are required for the enhanced cardiomyocyte number expansion induced by transient AT7519 treatment.

Discussion

Resolving inflammation is a promising therapeutic approach to promote tissue repair/regeneration following injury. CDK9 inhibitor compounds, currently deployed in clinical trials as anti-cancer treatments, can be applied experimentally to curtail early neutrophilic inflammation (Rossi et al., 2006; Lucas et al., 2014; Hoodless et al., 2016 and Cartwright et al., 2019). This study is the first to examine the effect of CDK9 inhibitors (AT7519 and FVP) during the inflammatory and regenerative response following tissue injury *in vivo*. Using a larval zebrafish model of cardiac injury combined with heartbeat-synchronised imaging, we showed that AT7519 and FVP resolve neutrophilic inflammation at the injured heart via reverse migration, but differentially regulate macrophage polarisation and myocardial regeneration.

As previously shown in various models of injury and infection *in vivo* (Rossi et al., 2006; Loynes et al., 2010; Leitch et al., 2012; Lucas et al., 2014; Hoodless et al., 2016 and Barth et al., 2020), we found CDK9 inhibitors to enhance the resolution of neutrophilic inflammation following heart injury in larval zebrafish. Numerous studies have demonstrated that CDK9 inhibitors induce neutrophil apoptosis via downregulation of Mcl-1 (Moulding et al., 1998; Rossi, et al., 2006; Leitch et al., 2012; Wang et al., 2012; Lucas et al., 2014 and Dorward et al., 2017). Here, we show that AT7519 and FVP promote the resolution of neutrophilic inflammation from the cardiac lesion *via* reverse migration (Figure 1). Despite previously observing increased neutrophil apoptosis following tail fin transection with CDK9i treatment (Hoodless et al., 2016), we did not find any evidence of this at the injured heart. Reverse migration is the primary inflammatory-cell resolution mechanism in this model (Kaveh et al., 2020), most likely due to the size and sterility of the myocardial laser wound. An injury of such scale would release fewer chemoattractant signals such as reactive oxygen species (e.g., hydrogen peroxide), cytokines (e.g., il-1β*)* and chemokines (e.g., cxcr2/cxcl8) responsible for regulating neutrophil wound retention (Yoo et al., 2011; Yan et al., 2014; Powell et al., 2017; Coombs et al., 2019; Isles et al., 2019). Expression of these inflammatory mediators could indeed be modulated in the presence of AT7519 or FVP, as documented in other studies (Santo et al., 2010 and Yik et al., 2014). Consequently, this would alter the chemoattractant gradient, desensitising wound-swarming neutrophils and inducing their reverse migration. Similarly, other compounds that cause neutrophil apoptosis in mammalian systems have been shown to promote neutrophil reverse migration following tail fin wounding in larval zebrafish (Robertson et al., 2014). Further research is needed to better understand how CDK9 inhibitors regulate the aforementioned inflammatory mediators to induce immune cell reverse migration, particularly via chemokine signaling at sites of

sterile injury (Isles et al., 2019 and Coombs et al., 2019). Reverse migration may well be an important neutrophil resolution mechanism following cardiac injury in mammals, as shown following sterile liver injury (Wang et al., 2017). However, with live imaging proving extremely difficult in mammalian models of MI, it is not currently possible to non-invasively visualise inflammatory cells at high spatiotemporal resolution.

The majority of CDK9 inhibitors act by competitively inhibiting the ATP-binding domain which is conserved between all CDKs (Krystof et al., 2012). Consequently, long-term exposure to CDK9 inhibitor compounds can cause undesirable effects due to inhibition of other CDKs, many of which are cell-cycle regulators, such as CDK2 (Azevedo et al., 1996 and Wyatt et al., 2008). We showed that continuous AT7519 or FVP treatments result in developmental and injury-associated adverse effects including reduced cardiomyocyte number expansion, ventricular ejection fraction, macrophage wound retention and neutropenia (Figure 2). Continuous FVP treatment has previously been shown to inhibit cardiomyocyte proliferation in larval zebrafish (Matrone et al., 2015), suggesting the same anti-proliferative effect could be occurring, although cardiomyocyte apoptosis may also contribute to the reduction in cardiomyocyte numbers. We postulated whether the adverse effects associated with continuous CDK9i treatment were due to non-specific binding. To test this, we developed a larval zebrafish CDK9 inhibitor selectivity assay using homozygous knockout *cdk9* mutants and heart rate as a surrogate measurement for overall health. The assay revealed that AT7519 and FVP accelerate the decline of heart rate in knockout mutants from one-day post treatment (Figure 4). This reduction in heart rate coincides with the onset of adverse phenotypes (Figure 2), indicating that from one-day post treatment both compounds were acting in a Cdk9-independent manner. However, the assay does not rule out the adverse effects being partially Cdk9-dependent, as vehicle-treated knockout mutants also displayed a decline in health, albeit more gradual. Of the two CDK9 inhibitors, FVP showed marked off-target effects in the selectivity assay (Figure 4), a likely cause for the prominent adverse phenotypes observed (Figure 2), which has also been reported *in vitro* (Garriga et al., 2010 and Liu et al., 2011). Indeed, this larval zebrafish knockout screening approach could be applied to other druggable targets and used to identify uniquely selective inhibitors in a high throughput manner and across short timescales (≤2 hours) *in vivo*.

By limiting the CDK9i treatment period to a two-hour window, we were able to enhance the resolution of neutrophilic inflammation while avoiding all adverse effects. Using the transient treatment wound macrophage accumulation was unaffected (Figure 3), suggesting that prolonged neutrophil swarming is not required for macrophage recruitment/retention. Furthermore, we observed an unexpected difference between CDK9i treatments where

AT7519, but not FVP, increased the polarisation of wound macrophages to a *tnf*$^{+}$ phenotype (Figure 3). The selectivity assay revealed that from two hours post treatment (the duration of transient treatment), FVP exhibited significantly less Cdk9 selectivity compared to AT7519 (Figure 4). Additionally, FVP has been shown to inhibit TNF activation and signaling in other models of inflammation (Takada et al., 2004; Haque et al., 2011 and Schmerwitz et al., 2011), whereas AT7519 does not disrupt TNF activity (Lucas et al., 2014). Overall, these findings suggest that FVP suppressed *tnf* upregulation in wound-associated macrophages. As our selectivity assay enables high throughput assessment of individual animals across short time scales live *in vivo*, it is not suited for gene expression analysis. Therefore, how AT7519 and FVP differentially influence the expression of inflammatory response genes could be further investigated by RNA sequencing.

Cellular mechanisms regulating immune cell activity after wounding have been largely characterised in murine models and are not entirely recapitulated in zebrafish. For example, neutrophil apoptosis, subsequent macrophage efferocytosis and polarisation have not been reported following wounding in larval zebrafish (Starnes and Huttenlocher, 2012; Robertson et al., 2014; Loynes et al., 2018 and Kaveh et al., 2020). Instead, the role of immune cells is more dynamic and closely coupled to molecular signaling (Loynes et al., 2018; Coombs et al., 2019; Tsarouchas et al., 2018 and Sanz-Morejon et al., 2019). Larval zebrafish studies have described *tnf*$^{+}$ macrophages to have pro-regenerative roles following tissue wounding (Nguyen-Chi et al., 2017; Tsarouchas et al., 2018; Gurevich et al., 2018 and Cavone et al., 2021). Our data show that cardiac-injured larvae transiently treated with AT7519, but not FVP, exhibit enhanced cardiomyocyte number expansion at two-days post injury (Figure 5), one day after the peak *tnf*$^{+}$ macrophage response (Figure 3). Importantly, we found macrophages to be required for the improved regenerative response following AT7519 treatment (Figure 6). One molecular mechanism for this macrophage-dependent effect could be that *tnf*$^{+}$ macrophages express/secrete mitogenic factors, such as *vegf*, as is the case during muscle wounding angiogenesis (Gurevich et al., 2018). Similarly, *tnf* itself could act as a mitogen via activation of histone genes in progenitor cells, as described during spinal cord regeneration (Cavone et al., 2021). Single-cell RNA sequencing of wound-dwelling macrophages has recently been performed in the spinal cord and skeletal musculature of larval zebrafish by Cavone et al. (2021) and Ratnayake et al. (2021) respectively. In both studies the pro-regenerative macrophage subpopulation identified expresses traditional M1 and M2 markers and shares mitogenic factors, specifically *tnf* and *hbegf* (Cavone et al., 2021 and Ratnayake et al., 2021). Whilst *tnf*$^{+}$ macrophages have pro-regenerative properties in larval zebrafish, *tnf* is likely one of many differentially regulated genes in macrophages that could be promoting cardiomyocyte regeneration in our model. Interestingly, in adult

zebrafish *tnf*$^{+}$ macrophages promote scar deposition following cardiac injury (Bevan et al., 2020), suggesting a transition in *tnf*$^{+}$ macrophage function during zebrafish development.

Our data indicate that increased cardiomyocyte number expansion following transient AT7519 treatment correlates with accelerated myocardial wound closure, to the point of almost complete regeneration (Figure 5). This was not, however, associated with enhanced cardiac function, which recovered rapidly in both AT7519-treated and control larvae. Cardiomyocyte proliferation is a prerequisite for cardiac regeneration in many animal models (Godwin et al., 2017; Chablais et al., 2011; Curado et al., 2007; Porrello et al., 2013), suggesting that cardiomyocyte proliferation, enhanced by macrophages in our model, could be driving myocardial wound closure. Furthermore, 4D LSFM imaging during myocardial regeneration revealed that wound-bordering cardiomyocytes protrude into and subsequently bridge across the wound, gradually sealing it (Figure 5 and Supplementary Video 7). Cardiomyocyte bridging has previously been reported following transplantation of neonatal rat cardiomyocytes to infarcted hearts *in vitro* (Sekine et al., 2006), however to our knowledge, this is the first time such an event has been observed live in the beating heart. Extracellular matrix proteins, such as collagen, could form a scaffold to facilitate cardiomyocyte wound bridging, as similar mechanisms occur in the injured hearts of adult zebrafish (Simoes et al., 2020). Future studies could perform high resolution live imaging and complementary sequencing experiments in larval zebrafish to unravel the cardiac/immune cell types and signaling molecules regulating cardiac regeneration.

As our findings are from a developing zebrafish model, it will be important to validate AT7519 treatment in an adult MI model that more closely mimics human disease. It will be particularly important to corroborate our novel findings by determining whether AT7519 polarises macrophages to a reparative phenotype and how this regulates cardiac fibrosis, function, scar resolution, and angiogenesis. Furthermore, it will be necessary to identify whether AT7519 affects other immune cell types absent in our model. Namely monocytes, B cells, T cells and eosinophils – all of which play important roles during myocardial injury and repair (Hofmann and Frantz, 2015 and Toor et al., 2017). Nevertheless, we have shown that timing, duration and selectivity of CDK9 inhibitor treatment is imperative when targeting the acute inflammatory response to promote tissue repair/regeneration. AT7519 treatment could be particularly effective in a clinical setting where MI is followed by prolonged coronary reperfusion injury, as there is a profound secondary influx of neutrophils (Vinten-Johansen, 2004; Niccoli et al., 2009 and Mangold et al., 2015). This can occur following percutaneous coronary intervention (PCI), a standard clinical procedure for opening an acutely occluded coronary artery following MI. Thus, AT7519 could be administered at the time of PCI to

resolve locally recruited neutrophils and promote downstream mechanisms that positively modulate myocardial repair.

In summary, we have shown that AT7519 and FVP resolve neutrophil infiltration by inducing reverse migration from the cardiac injury site. However, AT7519, unlike FVP, showed promise as a selective CDK9 inhibitor by augmenting macrophage polarisation and promoting cardiomyocyte regeneration. As such, future research should establish whether selective CDK9 inhibitors, such as AT7519, have analogous reparative effects on macrophage polarisation and infarct healing in adult models of MI associated with neutrophilic inflammation. This could ultimately reveal the clinical potential of selective CDK9 inhibition as an immunomodulatory therapy for myocardial infarction.

Materials and methods

Zebrafish husbandry and lines used

Zebrafish husbandry and maintenance was conducted as per standard operating procedures. This was in accordance with the Animals (Scientific Procedures) Act, 1986 and approved by The University of Edinburgh Animal Welfare and Ethical Review Board in a United Kingdom Home Office-approved establishment. All experiments were performed on staged animals aged between 3 dpf and 5 dpf (Kimmel et al., 1995). The following zebrafish lines were used: *Tg(myl7:eGFP)*^{twu26} (Huang et al., 2003), *Tg(mpx:mCherry)*^{uwm7} (Yoo et al., 2010), *Tg(mpeg1:mCherry)*^{gl23} (Ellett et al., 2011), *Tg(myl7:DsRed2-NLS)*^{f2} (Rottbauer et al., 2002), *Tg(TNFa:eGFP)*^{sa43296} (Nguyen-Chi et al., 2015), *Tg(myl7:h2b-GFP)*^{zf52} (Mickoleit et al., 2014), *cdk9*^{ed9} mutant (Hoodless et al., 2016) and *irf8*$^{st59/st95}$ mutant (Shiau et al., 2015). Adults were bred to yield desired combinations of transgenes in embryos. Embryos were treated with 0.003% phenylthiourea (Fisher Scientific) dissolved in conditioned water at 7 hpf to prevent pigment formation and enhance image clarity (Karlsson et al., 2001). Embryos and larvae were housed at 28.5°C in conditioned water and imaged at room temperature (23°C) using epifluorescence or light sheet fluorescence microscopy (details below). When necessary, larvae were periodically anesthetized using 40 µg/ml tricaine methanesulfonate (Sigma Aldrich) in conditioned water.

Cardiac injury

The hearts of 72 hpf larval zebrafish were precisely injured using a Zeiss Photo Activated Laser Microdissection (PALM) system, as previously described (Taylor et al., 2019 and Kaveh et al., 2020). Individual anaesthetised larvae were pipetted onto a glass slide in 20µl anesthetised conditioned water and laterally oriented so that the head is pointing leftward. Larvae were positioned adjacent to each other and navigated on the slide using the automated PALM controls. The laser was focussed specifically on the ventricular apex and subsequently fired through a 20X objective. Hearts were typically laser pulsed three times along the ventricular apex (Figure 2–supplement 1A) until ventricular contractility had diminished, the apex had shrunk, and the myocardial wall had swollen. Cardiac ruptured larvae that displayed pericardial bleeding following laser injury were appropriately disregarded. Larvae were deemed injured if they displayed a loss of fluorescent myocardial transgenic signal and/or a robust immune cell recruitment response at the cardiac injury site. Uninjured (control) larvae were treated in the same manner up to the point of laser injury, when they were separated and maintained in the same environmental conditions as injured fish.

Pharmacological CDK9 inhibitor treatment

Larvae were incubated in AT7519 (Astex Pharmaceuticals), Flavopiridol or DMSO vehicle (both Sigma Aldrich) dissolved in PTU-treated conditioned water at the following concentrations: 1μM or 50μM AT7519, 1μM or 3μM Flavopiridol, and/or 0.1% or 0.3% DMSO vehicle from 72 hpf or 4 hpi, depending on the experiment as indicated. For continuous treatments, larvae were incubated in drug or vehicle from 4 hpi until 24 hpi or 48 hpi. For transient treatments, larvae were incubated in drug or vehicle from 4 hpi until 6 hpi, at which point they were transferred to fresh conditioned water. For serial timepoint experiments, individual larvae were incubated per well of a 48-well plate containing 500μl of CDK9 inhibitor or DMSO vehicle in conditioned water. During these experiments, larvae were briefly removed for imaging at 6 hpi, 24 hpi or 48 hpi. For LSFM timelapse experiments, individual anesthetised larvae were embedded in 1% low melting point agarose (ThermoFisher) in conditioned water containing 50μM AT7519, 3μM Flavopiridol or DMSO vehicle within FEP tubes (Adtech Polymer Engineering). During LSFM timelapse imaging, larvae were continually anaesthetised using tricaine methanesulfonate conditioned water containing 50μM AT7519, 3μM Flavopiridol or DMSO vehicle, as appropriate for up to 24 hours.

Epifluorescence microscopy

A Leica M205 FA stereomicroscope with standard GFP and mCherry filters were used for serial timepoint imaging experiments. To visualise immune cells or record ventricular ejection fraction, larvae were anesthetised and mounted laterally on a glass slide in 50μl conditioned water. Immune cell numbers on the ventricle were quantified by counting neutrophils or macrophages moving synchronously with the beating heart, as performed previously (Kaveh et al., 2020). Cardiac images were acquired using a 16X objective and whole-body images were acquired using a 2.5X objective.

Heartbeat-synchronised light sheet fluorescence microscopy (LSFM)

Optically gated (heartbeat-synchronised) LSFM imaging methods have been thoroughly described and published by our group (Taylor et al., 2019 and Kaveh et al., 2020). Briefly, bespoke synchronisation software coupled with LSFM allows real-time 3D fluorescence imaging of the beating heart every time the heart returns to the desired target phase of the cardiac cycle, while minimising phototoxicity and photobleaching (Taylor et al., 2019). As a result, the beating heart appears computationally “frozen”, allowing live examination of immune cell responses and cardiomyocyte regeneration following injury *in vivo*. Each heart stack has a z-plane spacing of 1μm. For timelapse imaging, the entire heart is scanned in 3D every 3 minutes for up to 24 hours.

CDK9 inhibitor selectivity assay

Knockout *cdk9* mutant zebrafish were previously generated and characterised by our group (Hoodless et al., 2016). As homozygous *cdk9* mutants are not viable at adulthood, adult heterozygous *cdk9* mutants were identified by genotyping (Hoodless et al., 2016) and incrossed, yielding a mendelian mix of wild-type (25%), heterozygous (50%) and homozygous (25%) mutant zebrafish embryos. Homozygous *cdk9* mutants are easily phenotypically distinguishable during larval stages (Figure 4A), which was confirmed by genotyping (Figure 4B). At 72 hpf, *cdk9* homozygous mutant larvae were phenotypically selected and treated with AT7519, FVP or DMSO vehicle, at the indicated doses. Following this, heart rate (beats/minute) was measured per larva by manually counting heartbeats per twelve seconds using a brightfield stereomicroscope and multiplying by five. This was performed between groups at 2 hpt, 6 hpt, 12 hpt, 24 hpt and 48 hpt as a proxy for overall health, allowing individual larvae to be assessed in real time. Larvae that did not display any heartbeat were regarded as dead.

Preparing homozygous *irf8* (macrophage-null) mutants

Adult homozygous *irf8* mutants were outcrossed to *Tg(myl7:h2b-GFP)* fish and the transgenic offspring were raised to adulthood. Adult heterozygous *irf8* mutants were further incrossed and the offspring raised to adulthood. Adult zebrafish arising the heterozygous *irf8* mutant incrosses were genotyped to identify wild-type, heterozygous or homozygous mutant *irf8* alleles. First adult fish were anaesthetised in 40 µg/ml tricaine methanesulfonate and a section of one tail fin lobe was resected using a sterile scalpel. Tail fin clips were digested to extract DNA using 10mg/ml of Proteinase K, incubating at 67°C for 1 hour. The digest was ended with a 95°C incubation for 15 minutes. The *irf8* allele was amplified from the extracted DNA by PCR using forward (ACATAAGGCGTAGAGATTGGACG) and reverse (GAAACATAGTGCGGTCCTCATCC) primers and REDTaq ReadyMix PCR Reaction Mix (Sigma Aldrich). The PCR product was then digested for 1 hour at 37°C using the *AvaI* restriction enzyme (New England Bioscience) and the product run on a 2% agarose gel to visualise digested DNA fragments. In wild-type fish, the *AvaI* restriction enzyme cut site in intact, thus the PCR product is digested to give two bands approximately 200 bp and 100 bp in size. In heterozygous mutant fish, the *AvaI* restriction enzyme partially digests the PCR product. In homozygous mutant fish, the *AvaI* restriction enzyme cut site is not present, thus the 286 bp PCR product is not digested. Confirmed wild-type and homozygous *irf8* mutant adults were separated for experimental incrossing.

Neutral red staining

Wild-type or homozygous *irf8* mutant larvae at 3 dpf were incubated in 5μg/mL neutral red (Thermo Fisher Scientific) in conditioned water for 1 hour in the dark at 28.5°C. Larvae were then washed twice in conditioned water, anaesthetised using 40 µg/ml tricaine methanesulfonate and imaged by brightfield microscopy on a Leica M205 FA stereomicroscope.

Image Analysis:

Unless otherwise stated, all images were prepared, processed and analysed using ImageJ (Fiji) software (National Institute of Health).

Temporal colour code

LSFM-acquired z-stacks of neutrophil or macrophage migration on injured hearts were processed as maximum intensity projections and temporally overlaid across the indicated timepoints. The 'Temporal-Color Code' Fiji tool was applied to the hyperstack such that each overlaid timepoint is a different hue, producing a single image which summarises immune cell migration on the injured heart.

Ventricular cardiomyocyte number

Individual LSFM-acquired z-stacks of *Tg(myl7:DsRed2-NLS)* or *Tg(myl7:h2b-GFP)* hearts was used to quantify the number of cardiomyocyte nuclei using the 'TrackMate' Fiji plugin. The following segmentation parameters were initially applied to each z-stack: 'LoG detector', 'Median filter' and 'Sub-pixel localisation' selected; 'Estimated blob diameter' = 6µm and 'Threshold' = 1. The threshold value was optimised per experiment until all cardiomyocyte nuclei were included. Atrial cardiomyocytes were subtracted from the total by x coordinate filtering to give a final ventricular cardiomyocyte count.

Ventricular ejection fraction

The hearts of *Tg(myl7:GFP)* larvae were imaged in real time at 30 fps using epifluorescence microscopy to capture points in the cardiac cycle when the ventricle was in diastole and systole. Ventricular area in diastole and systole was measured manually and ventricular ejection fraction (by area) was calculated using the formula: 100 × [(Diastolic Area – Systolic Area)/Diastolic Area] (Matrone et al., 2013).

Whole-body immune cell number

Whole-body epifluorescence images of *Tg(mpx:mCherry)* or *Tg(mpeg1:mCherry)* larvae were used to estimate global immune cell numbers in a semi-automated manner using a Fiji macro. Briefly, individual images were thresholded using the 'Yen' technique, converted to

binary and whole-body immune cell thresholded area was quantified. The area of three thresholded immune cells were measured at random. Whole-body immune cell threshold area was divided by the average immune cell area to estimate global immune cell numbers per larva.

Ventricular *tnf*$^{+}$ macrophage number

Individual LSFM-acquired z-stacks of *Tg(mpeg1:mcherry;TNFa:GFP)* hearts were processed as maximum intensity projections to visualise macrophages and *tnf* expression throughout the heart. The number of ventricular macrophages expressing *tnf* (above that of background levels) were counted. *Tg(mpeg1:mcherry)* larvae were used as a measure of background fluorescence and a negative control in this context.

Myocardial wound area

Individual LSFM-acquired z-stacks of *Tg(myl7:GFP)* injured hearts were 3D rendered using Imaris software (Bitplane) based on absolute intensity, suggested segmentation and rendering parameters. Rendered hearts were saved as separate images and imported into Fiji. The *myl7:GFP* negative area at the ventricular apex (visualised as a render-free hole in the myocardium) was manually traced around and quantified to give myocardial wound area (μm^2) (Figure 5D and 5E).

Randomisation and blinding

At the start of each experiment larvae were screened for the relevant fluorescent signals and then randomly allocated to different experimental groups. All analysis was performed blinded to treatment groups.

Statistical analysis

Graphs were curated and statistical analysis was performed using GraphPad Prism 9 software. The normal distribution of quantitative data was confirmed using the Shapiro-Wilk test and subsequently analysed using parametric or non-parametric tests, as appropriate. If normally distributed, data were analysed by One-way ANOVA or Two-way ANOVA followed by a multiple comparison *post hoc* test. If not normally distributed, data were analysed using the Mann–Whitney *U*-test. Error bars indicate standard error of the mean (SEM) or standard deviation (SD). All statistical tests, *p*-values and *n* numbers used are provided in figure legends.

Acknowledgements

We thank Astex Therapeutics, who kindly provided AT7519 as a gift. We thank Chris Lucas for useful discussions. We thank the BVS Aquatics Facility Staff for their expert animal care during the course of this study.

Author contributions

AK, AGR, and MAD conceived and designed the study. AK and FAB carried out all experiments and analysis. AK wrote the manuscript. FAB, MEMO, CST, JMT, JJM, AGR and MAD edited the manuscript. MAD, AGR and CST supervised the study. All authors contributed to the article and approved the submitted version.

Competing interests

No competing interests declared.

Funding

This work was funded by a Medical Research Scotland studentship (PhD-1049-2016), a British Heart Foundation CoRE award (RE/13/3/30183) and a Medical Research Council UK award (MR/K013386/1).

References

1. Anderson, Jeffrey L., and David A. Morrow. 'Acute Myocardial Infarction'. *The New England Journal of Medicine* 376, no. 21 (25 May 2017): 2053–64. https://doi.org/10.1056/NEJMra1606915.
2. Arruda-Olson, Adelaide M., Guy S. Reeder, Malcolm R. Bell, Susan A. Weston, and Véronique L. Roger. 'Neutrophilia Predicts Death and Heart Failure after Myocardial Infarction: A Community-Based Study'. *Circulation. Cardiovascular Quality and Outcomes* 2, no. 6 (November 2009): 656–62. https://doi.org/10.1161/CIRCOUTCOMES.108.831024.
3. Awan, Farrukh T., Jeffrey A. Jones, Kami Maddocks, Ming Poi, Michael R. Grever, Amy Johnson, John C. Byrd, and Leslie A. Andritsos. 'A Phase 1 Clinical Trial of Flavopiridol Consolidation in Chronic Lymphocytic Leukemia Patients Following Chemoimmunotherapy'. *Annals of Hematology* 95, no. 7 (June 2016): 1137–43. https://doi.org/10.1007/s00277-016-2683-1.
4. Barth, Nicole D., Ramon Subiros-Funosas, Lorena Mendive-Tapia, Rodger Duffin, Mario A. Shields, Jennifer A. Cartwright, Sónia Troeira Henriques, et al. 'A Fluorogenic Cyclic Peptide for Imaging and Quantification of Drug-Induced Apoptosis'. *Nature Communications* 11, no. 1 (12 August 2020): 4027. https://doi.org/10.1038/s41467-020-17772-7.
5. Bevan, Laura, Zhi Wei Lim, Byrappa Venkatesh, Paul R. Riley, Paul Martin, and Rebecca J. Richardson. 'Specific Macrophage Populations Promote Both Cardiac Scar Deposition and Subsequent Resolution in Adult Zebrafish'. *Cardiovascular Research* 116, no. 7 (1 June 2020): 1357–71. https://doi.org/10.1093/cvr/cvz221.
6. Cartwright, Jennifer A., Christopher D. Lucas, and Adriano G. Rossi. 'Inflammation Resolution and the Induction of Granulocyte Apoptosis by Cyclin-Dependent Kinase Inhibitor Drugs'. *Frontiers in Pharmacology* 10 (2019). https://doi.org/10.3389/fphar.2019.00055.
7. Cavone, Leonardo, Tess McCann, Louisa K. Drake, Erika A. Aguzzi, Ana-Maria Oprişoreanu, Elisa Pedersen, Soe Sandi, et al. 'A Unique Macrophage Subpopulation Signals Directly to Progenitor Cells to Promote Regenerative Neurogenesis in the Zebrafish Spinal Cord'. *Developmental Cell* 56, no. 11 (7 June 2021): 1617-1630.e6. https://doi.org/10.1016/j.devcel.2021.04.031.
8. Chablais, Fabian, Julia Veit, Gregor Rainer, and Anna Jaźwińska. 'The Zebrafish Heart Regenerates after Cryoinjury-Induced Myocardial Infarction'. *BMC Developmental Biology* 11, no. 1 (7 April 2011): 21. https://doi.org/10.1186/1471-213X-11-21.

9. Chen, E. X., S. Hotte, H. Hirte, L. L. Siu, J. Lyons, M. Squires, S. Lovell, S. Turner, L. McIntosh, and L. Seymour. 'A Phase I Study of Cyclin-Dependent Kinase Inhibitor, AT7519, in Patients with Advanced Cancer: NCIC Clinical Trials Group IND 177'. *British Journal of Cancer* 111, no. 12 (December 2014): 2262–67. https://doi.org/10.1038/bjc.2014.565.
10. Chia, Stanley, John T. Nagurney, David F. M. Brown, O. Christopher Raffel, Fabian Bamberg, Fred Senatore, Frans J. Th Wackers, and Ik-Kyung Jang. 'Association of Leukocyte and Neutrophil Counts with Infarct Size, Left Ventricular Function and Outcomes after Percutaneous Coronary Intervention for ST-Elevation Myocardial Infarction'. *The American Journal of Cardiology* 103, no. 3 (1 February 2009): 333–37. https://doi.org/10.1016/j.amjcard.2008.09.085.
11. Coombs, Caroline, Antonios Georgantzoglou, Hazel A. Walker, Julian Patt, Nicole Merten, Hugo Poplimont, Elisabeth M. Busch-Nentwich, et al. 'Chemokine Receptor Trafficking Coordinates Neutrophil Clustering and Dispersal at Wounds in Zebrafish'. *Nature Communications* 10, no. 1 (14 November 2019): 5166. https://doi.org/10.1038/s41467-019-13107-3.
12. Curado, Silvia, Ryan M. Anderson, Benno Jungblut, Jeff Mumm, Eric Schroeter, and Didier Y. R. Stainier. 'Conditional Targeted Cell Ablation in Zebrafish: A New Tool for Regeneration Studies'. *Developmental Dynamics: An Official Publication of the American Association of Anatomists* 236, no. 4 (April 2007): 1025–35. https://doi.org/10.1002/dvdy.21100.
13. Daseke, Michael J., Fritz M. Valerio, William J. Kalusche, Yonggang Ma, Kristine Y. DeLeon-Pennell, and Merry L. Lindsey. 'Neutrophil Proteome Shifts over the Myocardial Infarction Time Continuum'. *Basic Research in Cardiology* 114, no. 5 (15 August 2019): 37. https://doi.org/10.1007/s00395-019-0746-x.
14. De Azevedo, W. F., H. J. Mueller-Dieckmann, U. Schulze-Gahmen, P. J. Worland, E. Sausville, and S. H. Kim. 'Structural Basis for Specificity and Potency of a Flavonoid Inhibitor of Human CDK2, a Cell Cycle Kinase'. *Proceedings of the National Academy of Sciences of the United States of America* 93, no. 7 (2 April 1996): 2735–40. https://doi.org/10.1073/pnas.93.7.2735.
15. Deng, Qing, Sa Kan Yoo, Peter J. Cavnar, Julie M. Green, and Anna Huttenlocher. 'Dual Roles for Rac2 in Neutrophil Motility and Active Retention in Zebrafish Hematopoietic Tissue'. *Developmental Cell* 21, no. 4 (18 October 2011): 735–45. https://doi.org/10.1016/j.devcel.2011.07.013.
16. Dewald, Oliver, Guofeng Ren, Georg D. Duerr, Martin Zoerlein, Christina Klemm, Christine Gersch, Sophia Tincey, Lloyd H. Michael, Mark L. Entman, and Nikolaos G. Frangogiannis. 'Of Mice and Dogs: Species-Specific Differences in the Inflammatory

781 Response Following Myocardial Infarction'. *The American Journal of Pathology* 164, no.
782 2 (February 2004): 665–77. https://doi.org/10.1016/S0002-9440(10)63154-9.
783 17. Dewald, Oliver, Pawel Zymek, Kim Winkelmann, Anna Koerting, Guofeng Ren, Tareq
784 Abou-Khamis, Lloyd H. Michael, Barrett J. Rollins, Mark L. Entman, and Nikolaos G.
785 Frangogiannis. 'CCL2/Monocyte Chemoattractant Protein-1 Regulates Inflammatory
786 Responses Critical to Healing Myocardial Infarcts'. *Circulation Research* 96, no. 8 (29
787 April 2005): 881–89. https://doi.org/10.1161/01.RES.0000163017.13772.3a.
788 18. Dorward, David A., Jennifer M. Felton, Calum T. Robb, Thomas Craven, Tiina Kipari,
789 Timothy S. Walsh, Christopher Haslett, Kallirroi Kefala, Adriano G. Rossi, and
790 Christopher D. Lucas. 'The Cyclin-Dependent Kinase Inhibitor AT7519 Accelerates
791 Neutrophil Apoptosis in Sepsis-Related Acute Respiratory Distress Syndrome'. *Thorax*
792 72, no. 2 (February 2017): 182–85. https://doi.org/10.1136/thoraxjnl-2016-209229.
793 19. Ellett, Felix, Luke Pase, John W. Hayman, Alex Andrianopoulos, and Graham J.
794 Lieschke. 'Mpeg1 Promoter Transgenes Direct Macrophage-Lineage Expression in
795 Zebrafish'. *Blood* 117, no. 4 (27 January 2011): e49–56. https://doi.org/10.1182/blood-
796 2010-10-314120.
797 20. Epelman, Slava, Peter P. Liu, and Douglas L. Mann. 'Role of Innate and Adaptive
798 Immune Mechanisms in Cardiac Injury and Repair'. *Nature Reviews. Immunology* 15, no.
799 2 (February 2015): 117–29. https://doi.org/10.1038/nri3800.
800 21. Eyvazi, Shirin, Mohammad Saeid Hejazi, Homan Kahroba, Mozghan Abasi, Reza
801 Eghdam Zamiri, and Vahideh Tarhriz. 'CDK9 as an Appealing Target for Therapeutic
802 Interventions'. *Current Drug Targets* 20, no. 4 (2019): 453–64.
803 https://doi.org/10.2174/1389450119666181026152221.
804 22. Frangogiannis, Nikolaos G. 'Regulation of the Inflammatory Response in Cardiac
805 Repair'. *Circulation Research* 110, no. 1 (6 January 2012): 159–73.
806 https://doi.org/10.1161/CIRCRESAHA.111.243162.
807 23. Frangogiannis, Nikolaos G, C.Wayne Smith, and Mark L Entman. 'The Inflammatory
808 Response in Myocardial Infarction'. *Cardiovascular Research* 53, no. 1 (1 January 2002):
809 31–47. https://doi.org/10.1016/S0008-6363(01)00434-5.
810 24. Garlichs, C. D., S. Eskafi, I. Cicha, A. Schmeisser, B. Walzog, D. Raaz, C. Stumpf, et al.
811 'Delay of Neutrophil Apoptosis in Acute Coronary Syndromes'. *Journal of Leukocyte*
812 *Biology* 75, no. 5 (2004): 828–35. https://doi.org/10.1189/jlb.0703358.
813 25. Garriga, Judit, Hongbo Xie, Zoran Obradovic, and Xavier Graña. 'Selective Control of
814 Gene Expression by CDK9 in Human Cells'. *Journal of Cellular Physiology* 222, no. 1
815 (January 2010): 200–208. https://doi.org/10.1002/jcp.21938.
816 26. Godwin, J. W., R. Debuque, E. Salimova, and N. A. Rosenthal. 'Heart Regeneration in
817 the Salamander Relies on Macrophage-Mediated Control of Fibroblast Activation and the

Extracellular Landscape'. *Npj Regenerative Medicine* 2, no. 1 (27 July 2017): 1–11. https://doi.org/10.1038/s41536-017-0027-y.

27. Gurevich, David B, Charlotte E Severn, Catherine Twomey, Alexander Greenhough, Jenna Cash, Ashley M Toye, Harry Mellor, and Paul Martin. 'Live Imaging of Wound Angiogenesis Reveals Macrophage Orchestrated Vessel Sprouting and Regression'. *The EMBO Journal* 37, no. 13 (2 July 2018). https://doi.org/10.15252/embj.201797786.
28. Haque, Abedul, Naoki Koide, Imtiaz Iftakhar-E-Khuda, Abu Shadat Mohammod Noman, Erdenezaya Odkhuu, Battuvshin Badamtseren, Yoshikazu Naiki, Takayuki Komatsu, Tomoaki Yoshida, and Takashi Yokochi. 'Flavopiridol Inhibits Lipopolysaccharide-Induced TNF-α Production through Inactivation of Nuclear Factor-KB and Mitogen-Activated Protein Kinases in the MyD88-Dependent Pathway'. *Microbiology and Immunology* 55, no. 3 (2011): 160–67. https://doi.org/10.1111/j.1348-0421.2010.00304.x.
29. Hind, Laurel E., and Anna Huttenlocher. 'Neutrophil Reverse Migration and a Chemokinetic Resolution'. *Developmental Cell* 47, no. 4 (19 November 2018): 404–5. https://doi.org/10.1016/j.devcel.2018.11.004.
30. Hofmann, Ulrich, and Stefan Frantz. 'Role of Lymphocytes in Myocardial Injury, Healing, and Remodeling after Myocardial Infarction'. *Circulation Research* 116, no. 2 (16 January 2015): 354–67. https://doi.org/10.1161/CIRCRESAHA.116.304072.
31. Hoodless, Laura J., Christopher D. Lucas, Rodger Duffin, Martin A. Denvir, Christopher Haslett, Carl S. Tucker, and Adriano G. Rossi. 'Genetic and Pharmacological Inhibition of CDK9 Drives Neutrophil Apoptosis to Resolve Inflammation in Zebrafish in Vivo'. *Scientific Reports* 5 (11 November 2016): 36980. https://doi.org/10.1038/srep36980.
32. Hout, G. P. J. van, W. W. van Solinge, C. M. Gijsberts, M. P. J. Teuben, P. H. C. Leliefeld, M. Heeres, F. Nijhoff, et al. 'Elevated Mean Neutrophil Volume Represents Altered Neutrophil Composition and Reflects Damage after Myocardial Infarction'. *Basic Research in Cardiology* 110, no. 6 (14 October 2015): 58. https://doi.org/10.1007/s00395-015-0513-6.
33. Huang, Chiu-Ju, Chi-Tang Tu, Chung-Der Hsiao, Fong-Jou Hsieh, and Huai-Jen Tsai. 'Germ-Line Transmission of a Myocardium-Specific GFP Transgene Reveals Critical Regulatory Elements in the Cardiac Myosin Light Chain 2 Promoter of Zebrafish'. *Developmental Dynamics* 228, no. 1 (2003): 30–40. https://doi.org/10.1002/dvdy.10356.
34. Isles, Hannah M., Kimberly D. Herman, Anne L. Robertson, Catherine A. Loynes, Lynne R. Prince, Philip M. Elks, and Stephen A. Renshaw. 'The CXCL12/CXCR4 Signaling Axis Retains Neutrophils at Inflammatory Sites in Zebrafish'. *Frontiers in Immunology* 10 (2019). https://doi.org/10.3389/fimmu.2019.01784.
35. Jopling, Chris, Eduard Sleep, Marina Raya, Mercè Martí, Angel Raya, and Juan Carlos Izpisúa Belmonte. 'Zebrafish Heart Regeneration Occurs by Cardiomyocyte

Dedifferentiation and Proliferation'. *Nature* 464, no. 7288 (25 March 2010): 606–9. https://doi.org/10.1038/nature08899.

36. Karlsson, J., J. von Hofsten, and P. E. Olsson. 'Generating Transparent Zebrafish: A Refined Method to Improve Detection of Gene Expression during Embryonic Development'. *Marine Biotechnology* 3, no. 6 (November 2001): 522–27. https://doi.org/10.1007/s1012601-0053-4.
37. Kaveh, Aryan, Finnius A. Bruton, Charlotte Buckley, Magdalena E. M. Oremek, Carl S. Tucker, John J. Mullins, Jonathan M. Taylor, Adriano G. Rossi, and Martin A. Denvir. 'Live Imaging of Heart Injury in Larval Zebrafish Reveals a Multi-Stage Model of Neutrophil and Macrophage Migration'. *Frontiers in Cell and Developmental Biology* 8 (2020): 579943. https://doi.org/10.3389/fcell.2020.579943.
38. Kikuchi, Kazu, Jennifer E. Holdway, Andreas A. Werdich, Ryan M. Anderson, Yi Fang, Gregory F. Egnaczyk, Todd Evans, Calum A. MacRae, Didier Y. R. Stainier, and Kenneth D. Poss. 'Primary Contribution to Zebrafish Heart Regeneration by Gata4+ Cardiomyocytes'. *Nature* 464, no. 7288 (25 March 2010): 601–5. https://doi.org/10.1038/nature08804.
39. Kimmel, C. B., W. W. Ballard, S. R. Kimmel, B. Ullmann, and T. F. Schilling. 'Stages of Embryonic Development of the Zebrafish'. *Developmental Dynamics: An Official Publication of the American Association of Anatomists* 203, no. 3 (July 1995): 253–310. https://doi.org/10.1002/aja.1002030302.
40. Kithcart, Aaron, and Calum A. MacRae. 'Using Zebrafish for High-Throughput Screening of Novel Cardiovascular Drugs'. *JACC. Basic to Translational Science* 2, no. 1 (February 2017): 1–12. https://doi.org/10.1016/j.jacbts.2017.01.004.
41. Kryštof, Vladimír, Sonja Baumli, and Robert Fürst. 'Perspective of Cyclin-Dependent Kinase 9 (CDK9) as a Drug Target'. *Current Pharmaceutical Design* 18, no. 20 (July 2012): 2883–90. https://doi.org/10.2174/138161212800672750.
42. Lai, Shih-Lei, Rubén Marín-Juez, Pedro Luís Moura, Carsten Kuenne, Jason Kuan Han Lai, Ayele Taddese Tsedeke, Stefan Guenther, Mario Looso, and Didier YR Stainier. 'Reciprocal Analyses in Zebrafish and Medaka Reveal That Harnessing the Immune Response Promotes Cardiac Regeneration'. Edited by Marianne Bronner. *ELife* 6 (20 June 2017): e25605. https://doi.org/10.7554/eLife.25605.
43. Leitch, A. E., C. D. Lucas, J. A. Marwick, R. Duffin, C. Haslett, and A. G. Rossi. 'Cyclin-Dependent Kinases 7 and 9 Specifically Regulate Neutrophil Transcription and Their Inhibition Drives Apoptosis to Promote Resolution of Inflammation'. *Cell Death and Differentiation* 19, no. 12 (December 2012): 1950–61. https://doi.org/10.1038/cdd.2012.80.

44. Liu, Xiangrui, Shenhua Shi, Frankie Lam, Chris Pepper, Peter M. Fischer, and Shudong Wang. 'CDKI-71, a Novel CDK9 Inhibitor, Is Preferentially Cytotoxic to Cancer Cells Compared to Flavopiridol'. *International Journal of Cancer* 130, no. 5 (1 March 2012): 1216–26. https://doi.org/10.1002/ijc.26127.
45. Loynes, Catherine A., Jou A. Lee, Anne L. Robertson, Michael Jg Steel, Felix Ellett, Yi Feng, Bruce D. Levy, Moira K. B. Whyte, and Stephen A. Renshaw. 'PGE2 Production at Sites of Tissue Injury Promotes an Anti-Inflammatory Neutrophil Phenotype and Determines the Outcome of Inflammation Resolution in Vivo'. *Science Advances* 4, no. 9 (September 2018): eaar8320. https://doi.org/10.1126/sciadv.aar8320.
46. Loynes, Catherine A., Jane S. Martin, Anne Robertson, Daniel M. I. Trushell, Philip W. Ingham, Moira K. B. Whyte, and Stephen A. Renshaw. 'Pivotal Advance: Pharmacological Manipulation of Inflammation Resolution during Spontaneously Resolving Tissue Neutrophilia in the Zebrafish'. *Journal of Leukocyte Biology* 87, no. 2 (2010): 203–12. https://doi.org/10.1189/jlb.0409255.
47. Lucas, C. D., D. A. Dorward, M. A. Tait, S. Fox, J. A. Marwick, K. C. Allen, C. T. Robb, et al. 'Downregulation of Mcl-1 Has Anti-Inflammatory pro-Resolution Effects and Enhances Bacterial Clearance from the Lung'. *Mucosal Immunology* 7, no. 4 (July 2014): 857–68. https://doi.org/10.1038/mi.2013.102.
48. Luke, Jason J., David R. D'Adamo, Mark A. Dickson, Mary Louise Keohan, Richard D. Carvajal, Robert G. Maki, Elisa de Stanchina, Elgilda Musi, Samuel Singer, and Gary K. Schwartz. 'The Cyclin-Dependent Kinase Inhibitor Flavopiridol Potentiates Doxorubicin Efficacy in Advanced Sarcomas: Preclinical Investigations and Results of a Phase I Dose-Escalation Clinical Trial'. *Clinical Cancer Research: An Official Journal of the American Association for Cancer Research* 18, no. 9 (1 May 2012): 2638–47. https://doi.org/10.1158/1078-0432.CCR-11-3203.
49. Ma, Yonggang, Alan J. Mouton, and Merry L. Lindsey. 'Cardiac Macrophage Biology in the Steady-State Heart, the Aging Heart, and Following Myocardial Infarction'. *Translational Research*, In-Depth Review: Macrophage Polarization, 191 (1 January 2018): 15–28. https://doi.org/10.1016/j.trsl.2017.10.001.
50. Ma, Yonggang, Andriy Yabluchanskiy, and Merry L. Lindsey. 'Neutrophil Roles in Left Ventricular Remodeling Following Myocardial Infarction'. *Fibrogenesis & Tissue Repair* 6, no. 1 (3 June 2013): 11. https://doi.org/10.1186/1755-1536-6-11.
51. Mahadevan, D., R. Plummer, M. S. Squires, D. Rensvold, S. Kurtin, C. Pretzinger, T. Dragovich, et al. 'A Phase I Pharmacokinetic and Pharmacodynamic Study of AT7519, a Cyclin-Dependent Kinase Inhibitor in Patients with Refractory Solid Tumors'. *Annals of Oncology* 22, no. 9 (1 September 2011): 2137–43. https://doi.org/10.1093/annonc/mdq734.

52. Mangold Andreas, Alias Sherin, Scherz Thomas, Hofbauer Thomas M., Jakowitsch Johannes, Panzenböck Adelheid, Simon Daniel, et al. 'Coronary Neutrophil Extracellular Trap Burden and Deoxyribonuclease Activity in ST-Elevation Acute Coronary Syndrome Are Predictors of ST-Segment Resolution and Infarct Size'. *Circulation Research* 116, no. 7 (27 March 2015): 1182–92. https://doi.org/10.1161/CIRCRESAHA.116.304944.
53. Matrone, Gianfranco, Jonathan M. Taylor, Kathryn S. Wilson, James Baily, Gordon D. Love, John M. Girkin, John J. Mullins, Carl S. Tucker, and Martin A. Denvir. 'Laser-Targeted Ablation of the Zebrafish Embryonic Ventricle: A Novel Model of Cardiac Injury and Repair'. *International Journal of Cardiology* 168, no. 4 (9 October 2013): 3913–19. https://doi.org/10.1016/j.ijcard.2013.06.063.
54. Matrone, Gianfranco, Kathryn S. Wilson, Sana Maqsood, John J. Mullins, Carl S. Tucker, and Martin A. Denvir. 'CDK9 and Its Repressor LARP7 Modulate Cardiomyocyte Proliferation and Response to Injury in the Zebrafish Heart'. *Journal of Cell Science* 128, no. 24 (15 December 2015): 4560–71. https://doi.org/10.1242/jcs.175018.
55. Mickoleit, Michaela, Benjamin Schmid, Michael Weber, Florian O. Fahrbach, Sonja Hombach, Sven Reischauer, and Jan Huisken. 'High-Resolution Reconstruction of the Beating Zebrafish Heart'. *Nature Methods* 11, no. 9 (September 2014): 919–22. https://doi.org/10.1038/nmeth.3037.
56. Moulding, D. A., J. A. Quayle, C. A. Hart, and S. W. Edwards. 'Mcl-1 Expression in Human Neutrophils: Regulation by Cytokines and Correlation with Cell Survival'. *Blood* 92, no. 7 (1 October 1998): 2495–2502.
57. Nahrendorf, Matthias, Filip K. Swirski, Elena Aikawa, Lars Stangenberg, Thomas Wurdinger, Jose-Luiz Figueiredo, Peter Libby, Ralph Weissleder, and Mikael J. Pittet. 'The Healing Myocardium Sequentially Mobilizes Two Monocyte Subsets with Divergent and Complementary Functions'. *The Journal of Experimental Medicine* 204, no. 12 (26 November 2007): 3037–47. https://doi.org/10.1084/jem.20070885.
58. Nguyen-Chi, Mai, Béryl Laplace-Builhé, Jana Travnickova, Patricia Luz-Crawford, Gautier Tejedor, Georges Lutfalla, Karima Kissa, Christian Jorgensen, and Farida Djouad. 'TNF Signaling and Macrophages Govern Fin Regeneration in Zebrafish Larvae'. *Cell Death & Disease* 8, no. 8 (10 August 2017): e2979. https://doi.org/10.1038/cddis.2017.374.
59. Nguyen-Chi, Mai, Béryl Laplace-Builhe, Jana Travnickova, Patricia Luz-Crawford, Gautier Tejedor, Quang Tien Phan, Isabelle Duroux-Richard, et al. 'Identification of Polarized Macrophage Subsets in Zebrafish'. *ELife* 4 (8 July 2015): e07288. https://doi.org/10.7554/eLife.07288.

60. Niccoli, Giampaolo, Francesco Burzotta, Leonarda Galiuto, and Filippo Crea. ‘Myocardial No-Reflow in Humans’. *Journal of the American College of Cardiology* 54, no. 4 (21 July 2009): 281–92. https://doi.org/10.1016/j.jacc.2009.03.054.
61. Porrello, Enzo R., Ahmed I. Mahmoud, Emma Simpson, Brett A. Johnson, David Grinsfelder, Diana Canseco, Pradeep P. Mammen, Beverly A. Rothermel, Eric N. Olson, and Hesham A. Sadek. ‘Regulation of Neonatal and Adult Mammalian Heart Regeneration by the MiR-15 Family’. *Proceedings of the National Academy of Sciences of the United States of America* 110, no. 1 (2 January 2013): 187–92. https://doi.org/10.1073/pnas.1208863110.
62. Poss, Kenneth D., Lindsay G. Wilson, and Mark T. Keating. ‘Heart Regeneration in Zebrafish’. *Science* 298, no. 5601 (13 December 2002): 2188–90. https://doi.org/10.1126/science.1077857.
63. Powell, Davalyn, Sebastien Tauzin, Laurel E. Hind, Qing Deng, David J. Beebe, and Anna Huttenlocher. ‘Chemokine Signaling and the Regulation of Bidirectional Leukocyte Migration in Interstitial Tissues’. *Cell Reports* 19, no. 8 (23 May 2017): 1572–85. https://doi.org/10.1016/j.celrep.2017.04.078.
64. Ratnayake, Dhanushika, Phong D. Nguyen, Fernando J. Rossello, Verena C. Wimmer, Jean L. Tan, Laura A. Galvis, Ziad Julier, et al. ‘Macrophages Provide a Transient Muscle Stem Cell Niche via NAMPT Secretion’. *Nature* 591, no. 7849 (March 2021): 281–87. https://doi.org/10.1038/s41586-021-03199-7.
65. Ridker, Paul M, Brendan M. Everett, Tom Thuren, Jean G. MacFadyen, William H. Chang, Christie Ballantyne, Francisco Fonseca, et al. ‘Antiinflammatory Therapy with Canakinumab for Atherosclerotic Disease’. *New England Journal of Medicine* 377, no. 12 (21 September 2017): 1119–31. https://doi.org/10.1056/NEJMoa1707914.
66. Robertson, Anne L., Geoffrey R. Holmes, Aleksandra N. Bojarczuk, Joseph Burgon, Catherine A. Loynes, Myriam Chimen, Amy K. Sawtell, et al. ‘A Zebrafish Compound Screen Reveals Modulation of Neutrophil Reverse Migration as an Anti-Inflammatory Mechanism’. *Science Translational Medicine* 6, no. 225 (26 February 2014): 225ra29. https://doi.org/10.1126/scitranslmed.3007672.
67. Rossi, Adriano G., Deborah A. Sawatzky, Annemieke Walker, Carol Ward, Tara A. Sheldrake, Nicola A. Riley, Alison Caldicott, et al. ‘Cyclin-Dependent Kinase Inhibitors Enhance the Resolution of Inflammation by Promoting Inflammatory Cell Apoptosis’. *Nature Medicine* 12, no. 9 (September 2006): 1056–64. https://doi.org/10.1038/nm1468.
68. Rottbauer, Wolfgang, Andrew J. Saurin, Heiko Lickert, Xuetong Shen, C. Geoff Burns, Z. Galen Wo, Rolf Kemler, Robert Kingston, Carl Wu, and Mark Fishman. ‘Reptin and Pontin Antagonistically Regulate Heart Growth in Zebrafish Embryos’. *Cell* 111, no. 5 (27 November 2002): 661–72. https://doi.org/10.1016/s0092-8674(02)01112-1.

69. Rubinstein, Amy L. ‘Zebrafish Assays for Drug Toxicity Screening’. *Expert Opinion on Drug Metabolism & Toxicology* 2, no. 2 (1 April 2006): 231–40. https://doi.org/10.1517/17425255.2.2.231.
70. Santo, L., S. Vallet, T. Hideshima, D. Cirstea, H. Ikeda, S. Pozzi, K. Patel, et al. ‘AT7519, A Novel Small Molecule Multi-Cyclin-Dependent Kinase Inhibitor, Induces Apoptosis in Multiple Myeloma via GSK-3beta Activation and RNA Polymerase II Inhibition’. *Oncogene* 29, no. 16 (22 April 2010): 2325–36. https://doi.org/10.1038/onc.2009.510.
71. Sanz-Morejón, Andrés, Ana B. García-Redondo, Hanna Reuter, Inês J. Marques, Thomas Bates, María Galardi-Castilla, Andreas Große, et al. ‘Wilms Tumor 1b Expression Defines a Pro-Regenerative Macrophage Subtype and Is Required for Organ Regeneration in the Zebrafish’. *Cell Reports* 28, no. 5 (30 July 2019): 1296-1306.e6. https://doi.org/10.1016/j.celrep.2019.06.091.
72. Savill, John, Ian Dransfield, Chris Gregory, and Chris Haslett. ‘A Blast from the Past: Clearance of Apoptotic Cells Regulates Immune Responses’. *Nature Reviews Immunology* 2, no. 12 (December 2002): 965–75. https://doi.org/10.1038/nri957.
73. Schloss, Maximilian J., Michael Horckmans, Katrin Nitz, Johan Duchene, Maik Drechsler, Kiril Bidzhekov, Christoph Scheiermann, Christian Weber, Oliver Soehnlein, and Sabine Steffens. ‘The Time-of-Day of Myocardial Infarction Onset Affects Healing through Oscillations in Cardiac Neutrophil Recruitment’. *EMBO Molecular Medicine* 8, no. 8 (August 2016): 937–48. https://doi.org/10.15252/emmm.201506083.
74. Schmerwitz, Ulrike K., Gabriele Sass, Alexander G. Khandoga, Jos Joore, Bettina A. Mayer, Nina Berberich, Frank Totzke, et al. ‘Flavopiridol Protects against Inflammation by Attenuating Leukocyte-Endothelial Interaction via Inhibition of Cyclin-Dependent Kinase 9’. *Arteriosclerosis, Thrombosis, and Vascular Biology* 31, no. 2 (February 2011): 280–88. https://doi.org/10.1161/ATVBAHA.110.213934.
75. Schwab, Jan M., Nan Chiang, Makoto Arita, and Charles N. Serhan. ‘Resolvin E1 and Protectin D1 Activate Inflammation-Resolution Programmes’. *Nature* 447, no. 7146 (14 June 2007): 869–74. https://doi.org/10.1038/nature05877.
76. Sekine, Hidekazu, Tatsuya Shimizu, Seiichi Kosaka, Eiji Kobayashi, and Teruo Okano. ‘Cardiomyocyte Bridging between Hearts and Bioengineered Myocardial Tissues with Mesenchymal Transition of Mesothelial Cells’. *The Journal of Heart and Lung Transplantation: The Official Publication of the International Society for Heart Transplantation* 25, no. 3 (March 2006): 324–32. https://doi.org/10.1016/j.healun.2005.09.017.
77. Shiau, Celia E., Zoe Kaufman, Ana M. Meireles, and William S. Talbot. ‘Differential Requirement for Irf8 in Formation of Embryonic and Adult Macrophages in Zebrafish’.

PLOS ONE 10, no. 1 (23 January 2015): e0117513. https://doi.org/10.1371/journal.pone.0117513.

78. Simões, Filipa C., Thomas J. Cahill, Amy Kenyon, Daria Gavriouchkina, Joaquim M. Vieira, Xin Sun, Daniela Pezzolla, et al. 'Macrophages Directly Contribute Collagen to Scar Formation during Zebrafish Heart Regeneration and Mouse Heart Repair'. *Nature Communications* 11, no. 1 (30 January 2020): 600. https://doi.org/10.1038/s41467-019-14263-2.
79. Starnes, Taylor W., and Anna Huttenlocher. 'Neutrophil Reverse Migration Becomes Transparent with Zebrafish'. *Advances in Hematology* 2012 (12 July 2012): e398640. https://doi.org/10.1155/2012/398640.
80. Sundar, Vaishnavi, Sanjana Vimal, M. s. Sai Mithlesh, Anupam Dutta, Ramasamy Tamizhselvi, and Venkatraman Manickam. 'Transcriptional Cyclin-Dependent Kinases as the Mediators of Inflammation-a Review'. *Gene* 769 (15 February 2021): 145200. https://doi.org/10.1016/j.gene.2020.145200.
81. Swirski, Filip K., and Matthias Nahrendorf. 'Leukocyte Behavior in Atherosclerosis, Myocardial Infarction, and Heart Failure'. *Science* 339, no. 6116 (11 January 2013): 161–66. https://doi.org/10.1126/science.1230719.
82. Takada, Yasunari, and Bharat B. Aggarwal. 'Flavopiridol Inhibits NF-KappaB Activation Induced by Various Carcinogens and Inflammatory Agents through Inhibition of IkappaBalpha Kinase and P65 Phosphorylation: Abrogation of Cyclin D1, Cyclooxygenase-2, and Matrix Metalloprotease-9'. *The Journal of Biological Chemistry* 279, no. 6 (6 February 2004): 4750–59. https://doi.org/10.1074/jbc.M304546200.
83. Tardif, Jean-Claude, Simon Kouz, David D. Waters, Olivier F. Bertrand, Rafael Diaz, Aldo P. Maggioni, Fausto J. Pinto, et al. 'Efficacy and Safety of Low-Dose Colchicine after Myocardial Infarction'. *New England Journal of Medicine* 381, no. 26 (26 December 2019): 2497–2505. https://doi.org/10.1056/NEJMoa1912388.
84. Taylor, Jonathan M., Carl J. Nelson, Finnius A. Bruton, Aryan Kaveh, Charlotte Buckley, Carl S. Tucker, Adriano G. Rossi, John J. Mullins, and Martin A. Denvir. 'Adaptive Prospective Optical Gating Enables Day-Long 3D Time-Lapse Imaging of the Beating Embryonic Zebrafish Heart'. *Nature Communications* 10, no. 1 (15 November 2019): 5173. https://doi.org/10.1038/s41467-019-13112-6.
85. Toor, Iqbal S., Dominik Rückerl, Iris Mair, Rob Ainsworth, Marco Meloni, Ana-Mishel Spiroski, Cecile Benezech, et al. 'Eosinophil Deficiency Promotes Aberrant Repair and Adverse Remodeling Following Acute Myocardial Infarction'. *JACC: Basic to Translational Science* 5, no. 7 (1 July 2020): 665–81. https://doi.org/10.1016/j.jacbts.2020.05.005.

86. Tsarouchas, Themistoklis M., Daniel Wehner, Leonardo Cavone, Tahimina Munir, Marcus Keatinge, Marvin Lambertus, Anna Underhill, et al. 'Dynamic Control of Proinflammatory Cytokines Il-1β and Tnf-α by Macrophages in Zebrafish Spinal Cord Regeneration'. *Nature Communications* 9, no. 1 (7 November 2018): 4670. https://doi.org/10.1038/s41467-018-07036-w.
87. Vinten-Johansen, Jakob. 'Involvement of Neutrophils in the Pathogenesis of Lethal Myocardial Reperfusion Injury'. *Cardiovascular Research* 61, no. 3 (15 February 2004): 481–97. https://doi.org/10.1016/j.cardiores.2003.10.011.
88. Wang, Jing, Mokarram Hossain, Ajitha Thanabalasuriar, Matthias Gunzer, Cynthia Meininger, and Paul Kubes. 'Visualizing the Function and Fate of Neutrophils in Sterile Injury and Repair'. *Science* 358, no. 6359 (6 October 2017): 111–16. https://doi.org/10.1126/science.aam9690.
89. Wang, Keqing, Peter Hampson, Jon Hazeldine, Vladimir Krystof, Miroslav Strnad, Paul Pechan, and Janet M. 'Cyclin-Dependent Kinase 9 Activity Regulates Neutrophil Spontaneous Apoptosis'. *PLoS ONE* 7, no. 1 (19 January 2012). https://doi.org/10.1371/journal.pone.0030128.
90. Wyatt, Paul G., Andrew J. Woodhead, Valerio Berdini, John A. Boulstridge, Maria G. Carr, David M. Cross, Deborah J. Davis, et al. 'Identification of N-(4-Piperidinyl)-4-(2,6-Dichlorobenzoylamino)-1H-Pyrazole-3-Carboxamide (AT7519), a Novel Cyclin Dependent Kinase Inhibitor Using Fragment-Based X-Ray Crystallography and Structure Based Drug Design'. *Journal of Medicinal Chemistry* 51, no. 16 (1 August 2008): 4986–99. https://doi.org/10.1021/jm800382h.
91. Xu, Shisan, Fangjing Xie, Li Tian, Sinai Hc Manno, Francis A. M. Manno, and Shuk Han Cheng. 'Prolonged Neutrophil Retention in the Wound Impairs Zebrafish Heart Regeneration after Cryoinjury'. *Fish & Shellfish Immunology* 94 (November 2019): 447–54. https://doi.org/10.1016/j.fsi.2019.09.030.
92. Yan, Bo, Peidong Han, Lifeng Pan, Wei Lu, Jingwei Xiong, Mingjie Zhang, Wenqing Zhang, Li Li, and Zilong Wen. 'IL-1β and Reactive Oxygen Species Differentially Regulate Neutrophil Directional Migration and Basal Random Motility in a Zebrafish Injury-Induced Inflammation Model'. *Journal of Immunology* 192, no. 12 (15 June 2014): 5998–6008. https://doi.org/10.4049/jimmunol.1301645.
93. Yik, Jasper H. N., Zi'ang Hu, Ratna Kumari, Blaine A. Christiansen, and Dominik R. Haudenschild. 'Cyclin-Dependent Kinase 9 Inhibition Protects Cartilage from the Catabolic Effects of pro-Inflammatory Cytokines'. *Arthritis & Rheumatology* 66, no. 6 (June 2014): 1537–46. https://doi.org/10.1002/art.38378.
94. Yoo, Sa Kan, Qing Deng, Peter J. Cavnar, Yi I. Wu, Klaus M. Hahn, and Anna Huttenlocher. 'Differential Regulation of Protrusion and Polarity by PI3K during

Neutrophil Motility in Live Zebrafish'. *Developmental Cell* 18, no. 2 (16 February 2010): 226–36. https://doi.org/10.1016/j.devcel.2009.11.015.

Figure Legends

Figure 1: CDK9i treatment resolves neutrophil infiltration following cardiac injury by promoting reverse migration. (A) Experimental timeline indicating cardiac injury, CDK9i treatment and imaging timepoints. **(B)** Epifluorescence images of *Tg(myl7:GFP;mpx:mCherry)* larvae displaying neutrophil presence on the injured ventricle at 4 hpi (prior to treatment), and at 6 hpi and 24 hpi with 0.3% DMSO vehicle (top panel), 50μM AT7519 (middle panel) or 3μM FVP (bottom panel). White arrowhead indicates ventricular apex injury site marked by a loss of myocardial GFP and neutrophil accumulation. **(C)** Number of ventricular neutrophils at 4 hpi, 6 hpi and 24 hpi with 50μM AT7519 (top graph) or 3μM FVP (bottom graph) treatment. Error bars = SEM, n = 19 larvae, experimental n = 3. Two-way ANOVA and Bonferroni *post hoc* test performed for comparisons between cardiac-injured DMSO vehicle or CDK9i treatment groups where **** $p < 0.0001$. **(D)** LSFM images of neutrophil (*mpx:mCherry*) migration temporally colour coded between 4 hpi and 6 hpi with 0.1% DMSO vehicle (top) or 50μM AT7519 (bottom). Neutrophil positions appear as a different colour depending on the point in time (as indicated in the key). White dashed line indicates outline of ventricle. Arrowhead indicates starting position of neutrophil (DMSO vehicle) or ending position of neutrophils (AT7519) relative to image panels in **E** and **F** respectively. White arrowhead indicates ventricular apex injury site **(E)** LSFM timelapse-derived images of ventricular neutrophil migration with DMSO vehicle (0.1%), hpi indicated above each image. Blue arrowhead tracks an individual neutrophil migrating across the ventricular apex. **(F)** LSFM timelapse-derived images of neutrophil migration from ventricle to pericardium with AT7519 (50μM) treatment, hpi indicated above each image. Blue and green arrowheads track individual neutrophils reverse migrating anteriorly and posteriorly to the pericardium respectively. LSFM fluorescence images were acquired in 3D and maximum intensity projections were used for temporal colour code analysis (**D**) or are individually displayed (**E and F**). All scale bars = 50 μm.

Figure 2: Continuous CDK9i treatment reduces macrophage retention on the injured ventricle and impairs cardiomyocyte number expansion. (A) Experimental timeline indicating cardiac injury, continuous CDK9i treatment and imaging timepoints. **(B)** Number of ventricular macrophages at 4 hpi, 6 hpi, 24 hpi and 48 hpi with ≤0.3% DMSO vehicle, 50μM AT7519 (top graph) or 3μM FVP (bottom graph) treatment. Error bars = SEM, *n* = 16 larvae, experimental *n* = 3. Two-way ANOVA and Bonferroni *post hoc* test performed for comparisons between cardiac-injured DMSO vehicle or CDK9i treatment groups where ** $p < 0.01$, *** $p < 0.001$, and **** $p < 0.0001$. **(C)** LSFM timelapse-derived images of cardiac-injured *Tg(mpeg1:mCherry)* larvae displaying ventricular macrophage presence at 6 hpi (left panel) and 20 hpi (middle panel) with 0.3% DMSO vehicle or 3μM FVP. LSFM timelapse images of macrophage (*mpeg1:mCherry*) migration temporally colour coded with DMSO vehicle (0.3%) or FVP (3μM) treatment (right panel). Start and end timepoint (hpi) for colour code is indicated. White dashed line indicates outline of ventricle. White arrowhead indicates ventricular apex injury site **(D)** LSFM images of *Tg(myl7:DsRed2-NLS)* larvae displaying ventricular cardiomyocytes at 24 hours post treatment (hpt) and 48 hpt with 0.3% DMSO vehicle (top panel), 50μM AT7519 (middle panel) or 3μM FVP (bottom panel). **(E)** Number of ventricular cardiomyocytes at 24 hpt and 48 hpt with ≤0.3% DMSO vehicle, 50μM AT7519 (top graph) or 3μM FVP (bottom graph). Error bars = SD, *n* = 25 larvae, experimental *n* = 3. One-way ANOVA and Tukey *post hoc* test performed for comparisons between DMSO vehicle or CDK9i treatment groups where ** $p < 0.01$ and *** $p < 0.001$. LSFM fluorescence images were acquired in 3D and maximum intensity projections are used for timepoint display (**C and D**) or temporal colour code analysis (**C**). All scale bars = 50 μm.

Figure 3: Transient CDK9i treatment does not affect cardiac macrophage numbers and AT7519 enhances wound macrophage *tnf* polarisation following injury. (A) Experimental timeline indicating cardiac injury, transient CDK9i treatment and imaging timepoints. **(B)** LSFM images of *Tg(mpeg1:mCherry;TNFa:GFP)* larvae displaying macrophage accumulation and *tnf* expression on the injured ventricle at 24 hpi following transient treatment with 0.3% DMSO vehicle (top panel), 50μM AT7519 (middle panel) or 3μM FVP (bottom panel). White arrowhead indicates ventricular apex injury site. Number of ventricular macrophages **(C)** and ventricular *tnf*$^{+}$ macrophages **(D)** at 24 hpi and 48 hpi following transient AT7519 (50μM) treatment. **(E)** Number of ventricular macrophages (total and *tnf*$^{+}$) at 24 hpi following transient FVP (3μM) treatment. (**D and E**) Error bars = SD, *n* = 28 larvae, experimental *n* = 3. One-way ANOVA and Tukey *post hoc* test performed for comparisons between treatment groups where *** $p < 0.001$ and Ns, non-significant. **(F)** LSFM timelapse-derived images displaying macrophage migration and *tnf* expression on the injured ventricle, hpi indicated above each image. White arrowhead (top panel, all timepoints) tracks an individual *tnf*$^{+}$ macrophage (*mpeg1*^{low}) migrating to the ventricular apex. Blue arrowheads (top panel, at 15.00 hpi) indicate two macrophages that have upregulated their *tnf* expression at the injured ventricular apex. LSFM fluorescence images were acquired in 3D and maximum intensity projections are displayed. White dashed line indicates outline of ventricle. All scale bars = 50 μm.

Figure 4: AT7519 is a more selective CDK9 inhibitor than Flavopiridol in zebrafish. (A) Brightfield images of a *cdk9*$^{+/+}$ (top), *cdk9*$^{+/-}$ (middle) and *cdk9*$^{-/-}$ (bottom) whole zebrafish at 4 dpf. Scale bars = 1 mm. **(B)** Restriction enzyme digest gel displaying *cdk9* genotypes of zebrafish larvae. Hyperladder (HL) band and individual genotype bands (in order: *cdk9*$^{-/-}$, *cdk9*$^{+/-}$ and *cdk9*$^{+/+}$) are indicated. Heart rate (beats/min) **(C)** and survival % **(E)** of *cdk9*$^{-/-}$ larvae at 2 hpt, 6 hpt, 12 hpt, 24 hpt and 48 hpt with 0.1%, DMSO vehicle, 1μM AT7519 or 1μM FVP treatment. Heart rate (beats/min) **(D)** and survival % **(F)** of *cdk9*$^{-/-}$ larvae at 2 hpt, 6 hpt, 12 hpt, 24 hpt and 48 hpt with 0.3% DMSO vehicle, 50μM AT7519 or 3μM FVP treatment. **(C and D)** Error bars = SEM, *n* = 15 larvae, experimental *n* = 3. Two-way ANOVA and Bonferroni *post hoc* test performed for comparisons between DMSO vehicle or CDK9i treatment groups where ** $p < 0.01$, *** $p < 0.001$ and **** $p < 0.0001$.

Figure 5: Transient AT7519 treatment enhances cardiomyocyte number expansion and accelerates the rate of myocardial wound regeneration following injury. (A) Experimental timeline indicating cardiac injury, transient CDK9i treatment and imaging timepoints. **(B)** LSFM images of *Tg(myl7:DsRed2-NLS)* larvae displaying ventricular cardiomyocytes at 48 hpi following transient treatment with 0.3% DMSO vehicle (left panel), 50μM AT7519 (middle panel) or 3μM FVP (right panel). **(C)** Number of ventricular cardiomyocytes at 24 hpi and 48 hpi following transient treatment with ≤0.3% DMSO vehicle, 50μM AT7519 (left graph) or 3μM FVP (right graph). Error bars = SD, *n* = 29 larvae, experimental *n* = 3. One-way ANOVA and Tukey *post hoc* test performed for comparisons between DMSO vehicle or CDK9i treatment groups where ** $p < 0.01$. **(D)** Surface rendered LSFM image of a *Tg(myl7:GFP)* heart. White dashed line outlines the ventricular apex area that is subject to laser injury. **(E)** Surface rendered LSFM image of a *Tg(myl7:GFP)* wound at the ventricular apex at 24 hpi and 48 hpi, following transient treatment with 0.1% DMSO vehicle (top panel) or 50μM AT7519 (bottom panel). Arrowheads indicate cardiomyocyte protrusions adjacent to the wound (*myl7:GFP* negative). Scale bars = 20 μm. **(F)** Myocardial wound area (μm^2) at 24 hpi and 48 hpi following transient treatment with 0.1% DMSO vehicle or 50μM AT7519. Error bars = SD, *n* = 27 larvae, experimental *n* = 3. One-way ANOVA and Tukey *post hoc* test performed for comparisons between treatment groups. **(G)** Myocardial wound closure (%) between 24 hpi and 48 hpi following transient treatment with 0.1% DMSO vehicle or 50μM AT7519. Error bars = SD, *n* = 27 larvae, experimental *n* = 3. Mann–Whitney *U*-test performed for comparison between treatment groups where * $p < 0.05$. **(H)** Surface rendered LSFM timelapse-derived images of an injured *myl7:GFP* ventricle, hpi indicated. Arrowheads indicate myocardial wound (*myl7:GFP* negative). Asterisk indicates cardiomyocytes bridging across the myocardial wound (*myl7:GFP* negative). LSFM fluorescence images were acquired in 3D and maximum intensity projections **(B)** or 3D renders **(D, E and H)** are displayed. Unless stated, all scale bars = 50 μm. Ns, non-significant.

Figure 6: Macrophages are required for enhanced cardiomyocyte number expansion response following cardiac injury and transient AT7519 treatment. (A) Restriction enzyme digest gel displaying *irf8* zebrafish genotypes. Hyperladder (HL) band and individual genotype bands (in order: $irf8^{+/+}$,$irf8^{+/-}$ and $irf8^{-/-}$) are indicated. **(B)** Brightfield images of 3 dpf larval heads stained with neutral red showing macrophages/microglia in the brain of $irf8^{+/+}$ larvae but not in $irf8^{-/-}$ larvae, with $irf8^{-/-}$ larvae absent of all macrophages/microglia. Arrowheads indicate the presence of macrophages/microglia, black panel indicates magnified view. Scale bars = 500 μm. **(C)** LSFM images of $irf8^{+/+}$ and $irf8^{-/-}$ *Tg(myl7:h2b-GFP)* larvae displaying ventricular cardiomyocytes at 48 hpi following transient treatment with 0.1% DMSO vehicle (top panel) or 50μM AT7519 (bottom panel). Scale bar = 50 μm. **(D)** Number of ventricular cardiomyocytes at 48 hpi following transient treatment with 0.1% DMSO vehicle or 50μM AT7519 in $irf8^{+/+}$ and $irf8^{-/-}$ larvae. Error bars = SD, n = 25 larvae, experimental n = 3. One-way ANOVA and Tukey *post hoc* test performed for comparisons between DMSO vehicle or AT7519 treatment groups where * $p < 0.05$ and Ns, non-significant.

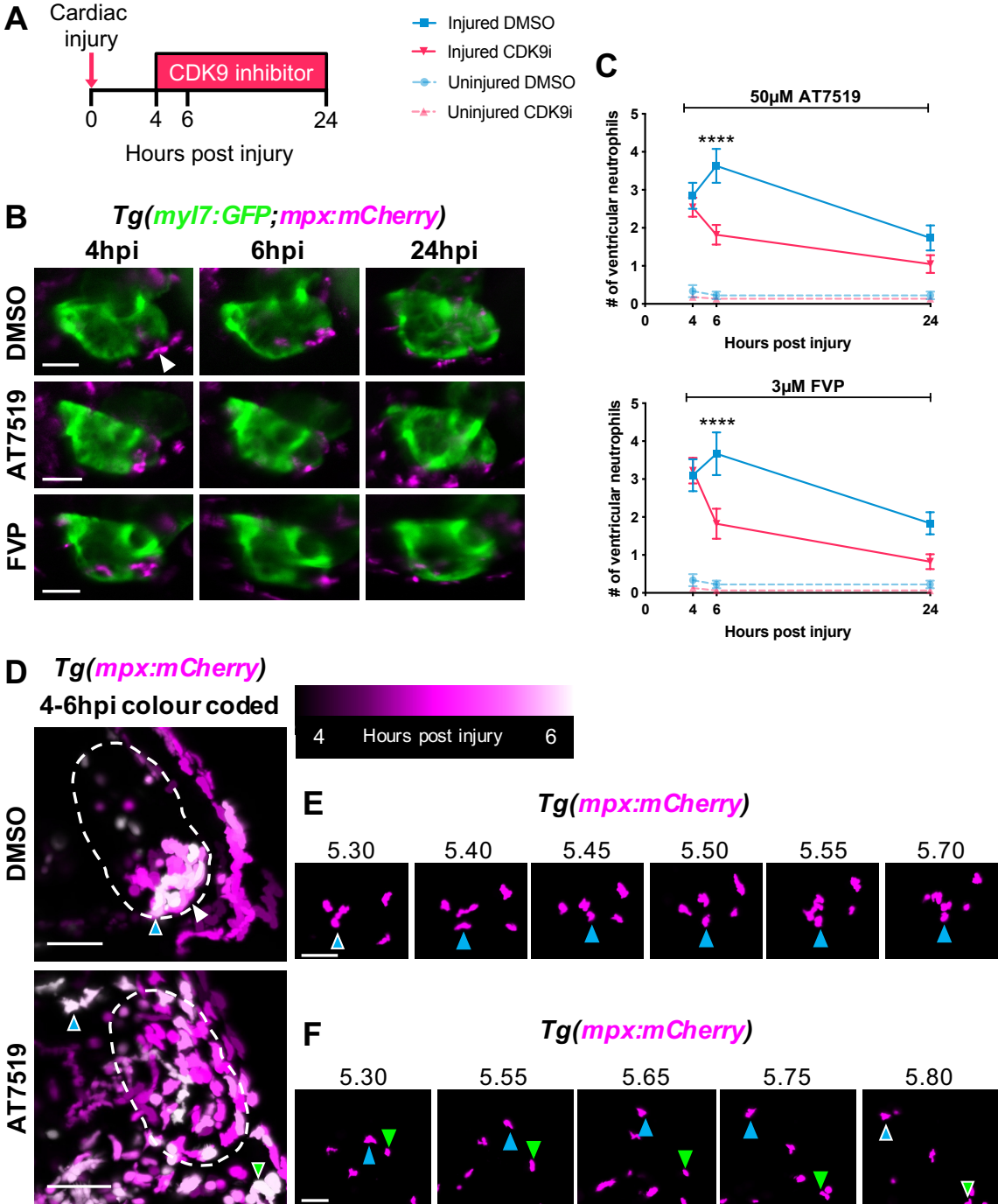
A
Cardiac injury
CDK9 inhibitor
0
4
6
24
Hours post injury
Injured DMSO
Injured CDK9i
Uninjured DMSO
Uninjured CDK9i
B
Tg(myl7:GFP;mpx:mCherry)
4hpi
6hpi
24hpi
DMSO
AT7519
FVP
C
50μM AT7519
****
# of ventricular neutrophils
Hours post injury
3μM FVP
****
# of ventricular neutrophils
Hours post injury
D
Tg(mpx:mCherry)
4-6hpi colour coded
4
Hours post injury
6
DMSO
AT7519
E
Tg(mpx:mCherry)
5.30
5.40
5.45
5.50
5.55
5.70
F
Tg(mpx:mCherry)
5.30
5.55
5.65
5.75
5.80

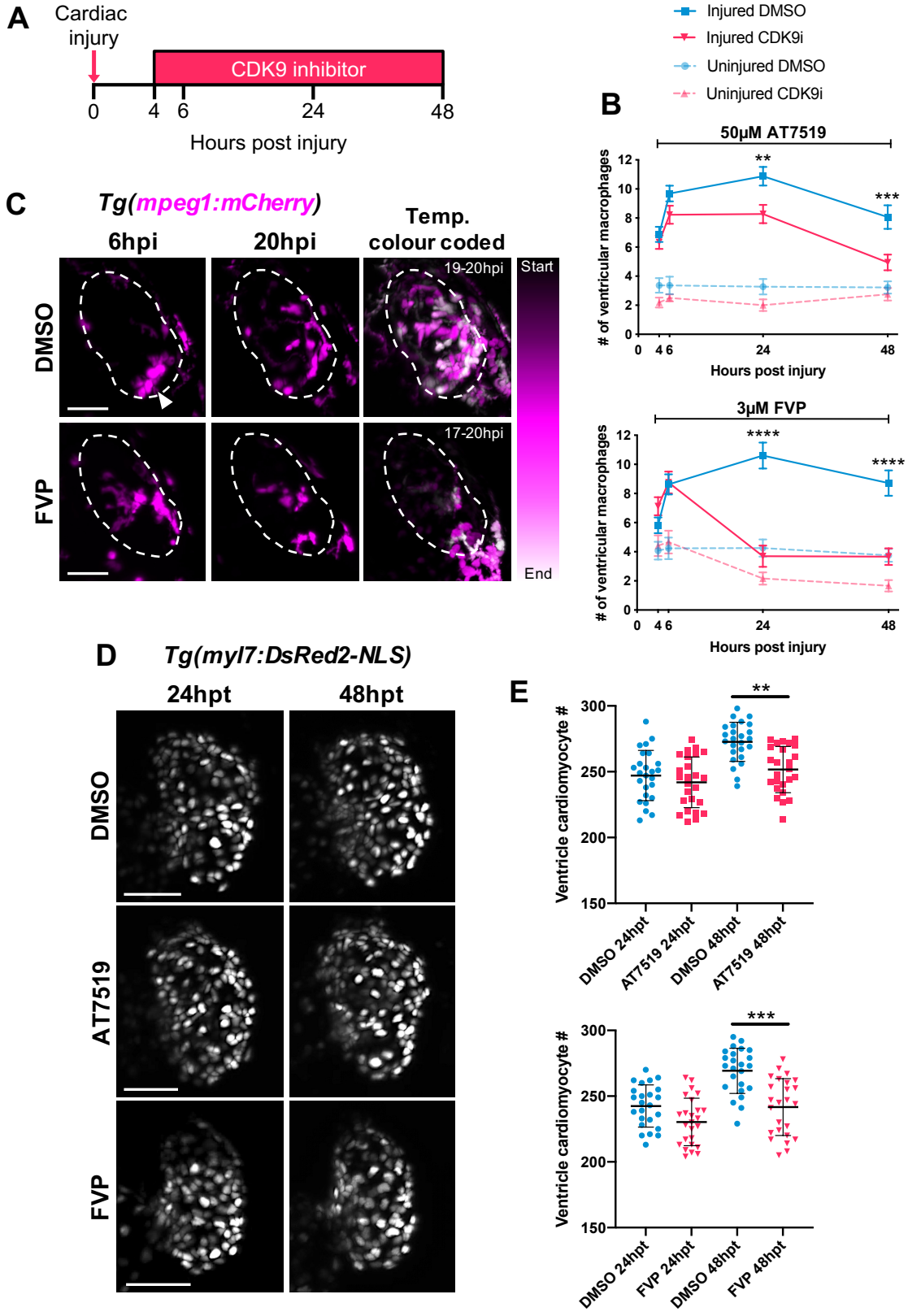
A
Cardiac injury
CDK9 inhibitor
0
4
6
24
48
Hours post injury
Injured DMSO
Injured CDK9i
Uninjured DMSO
Uninjured CDK9i
B
50μM AT7519
# of ventricular macrophages
Hours post injury
3μM FVP
C
Tg(mpeg1:mCherry)
6hpi
20hpi
Temp. colour coded
19-20hpi
17-20hpi
Start
End
DMSO
FVP
D
Tg(myl7:DsRed2-NLS)
24hpt
48hpt
DMSO
AT7519
FVP
E
Ventricle cardiomyocyte #
DMSO 24hpt
AT7519 24hpt
DMSO 48hpt
AT7519 48hpt
FVP 24hpt
FVP 48hpt

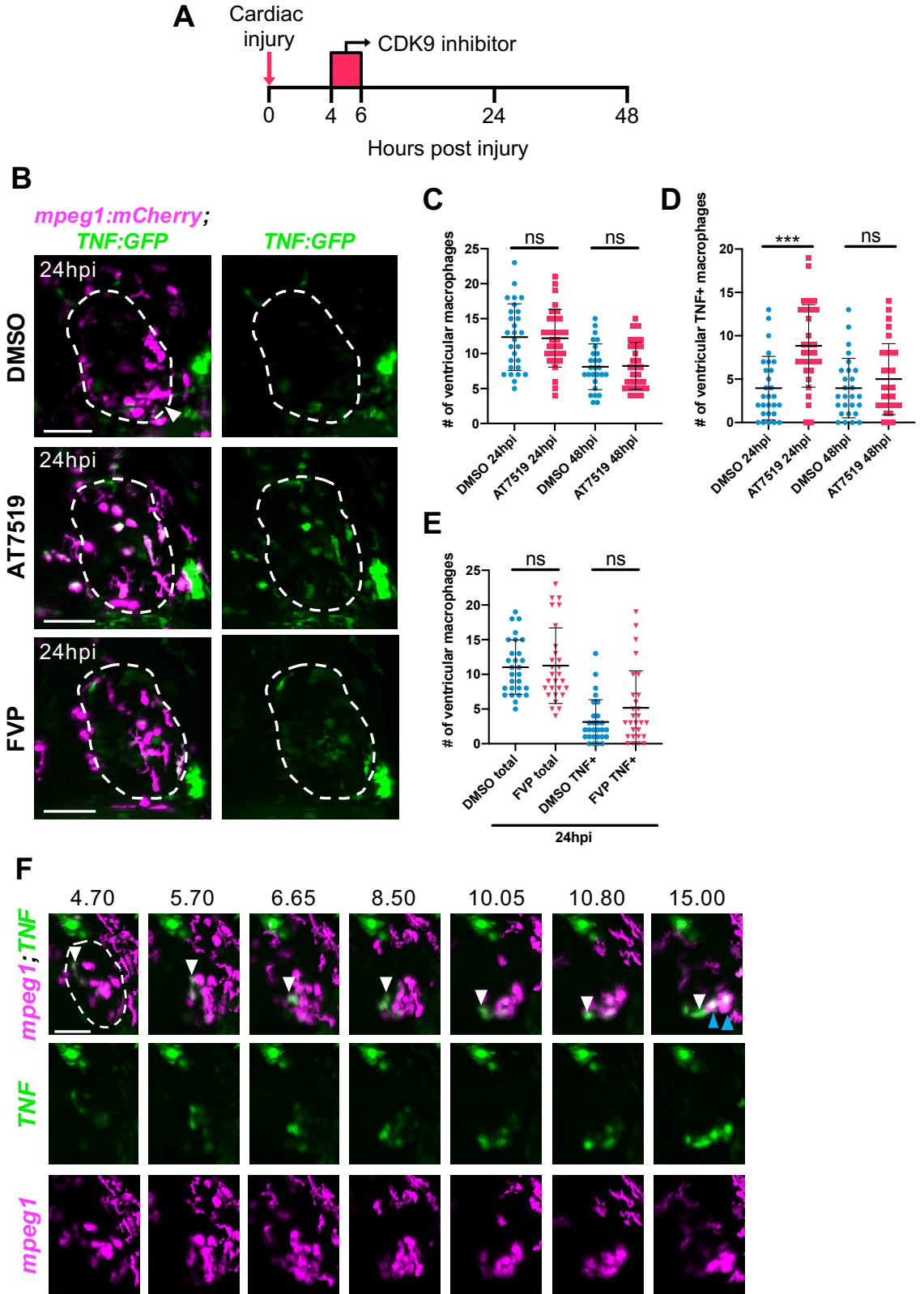
A
Cardiac injury
CDK9 inhibitor
0
4
6
24
48
Hours post injury
B
mpeg1:mCherry;
TNF:GFP
TNF:GFP
24hpi
DMSO
AT7519
FVP
C
# of ventricular macrophages
ns
ns
DMSO 24hpi
AT7519 24hpi
DMSO 48hpi
AT7519 48hpi
D
# of ventricular TNF+ macrophages
***
ns
E
# of ventricular macrophages
DMSO total
FVP total
DMSO TNF+
FVP TNF+
24hpi
F
4.70
5.70
6.65
8.50
10.05
10.80
15.00
mpeg1;TNF
TNF
mpeg1

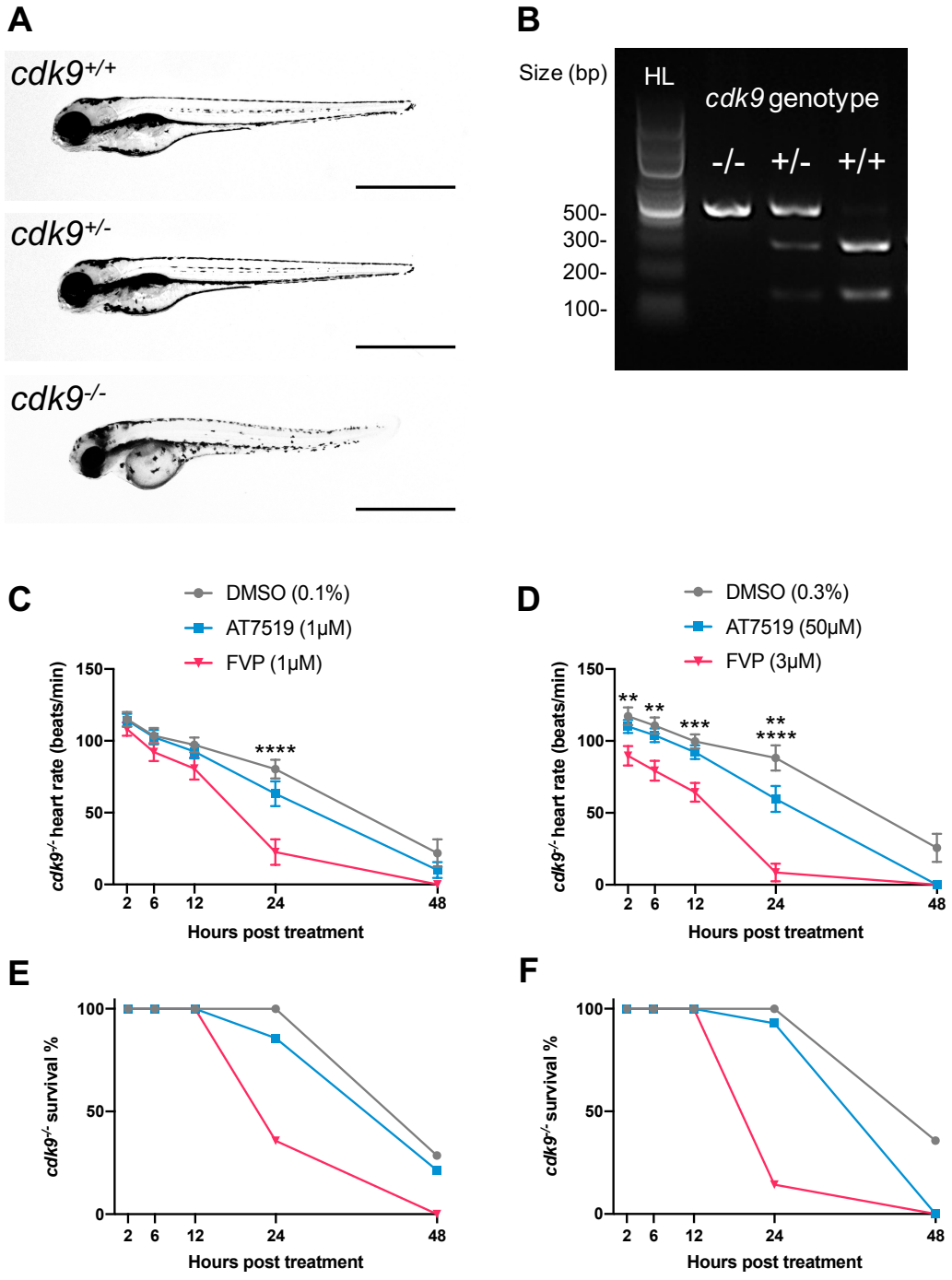
A
cdk9+/+
cdk9+/-
cdk9-/-
B
Size (bp)
HL
cdk9 genotype
-/-
+/-
+/+
500-
300-
200-
100-
C
DMSO (0.1%)
AT7519 (1μM)
FVP (1μM)
cdk9-/- heart rate (beats/min)
150
100
50
0
****
2
6
12
24
48
Hours post treatment
D
DMSO (0.3%)
AT7519 (50μM)
FVP (3μM)
cdk9-/- heart rate (beats/min)
**
**
***
**
****
Hours post treatment
E
cdk9-/- survival %
100
50
0
Hours post treatment
F
cdk9-/- survival %
Hours post treatment

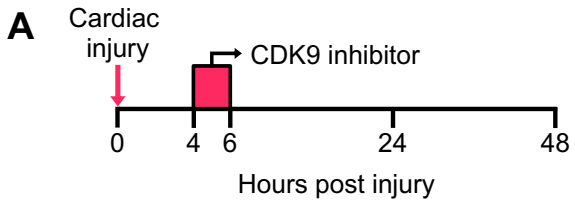
A
Cardiac injury
CDK9 inhibitor
0
4
6
24
48
Hours post injury

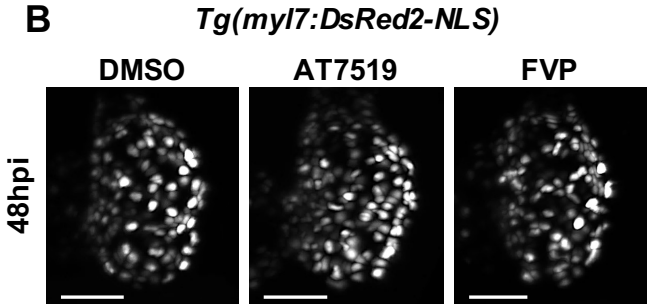
B
Tg(myl7:DsRed2-NLS)
DMSO
AT7519
FVP
48hpi

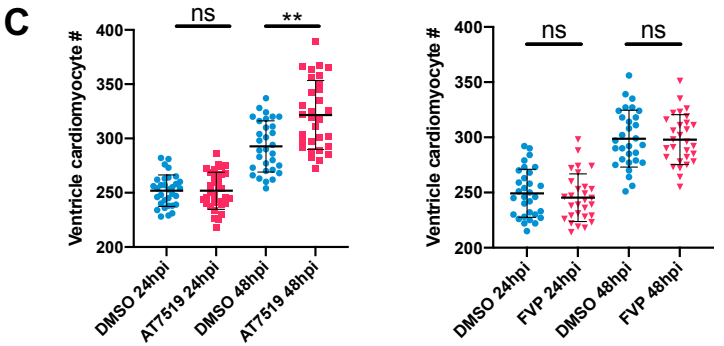
C
Ventricle cardiomyocyte #
ns
**
DMSO 24hpi
AT7519 24hpi
DMSO 48hpi
AT7519 48hpi
Ventricle cardiomyocyte #
ns
ns
DMSO 24hpi
FVP 24hpi
DMSO 48hpi
FVP 48hpi

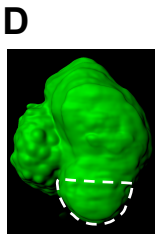
D

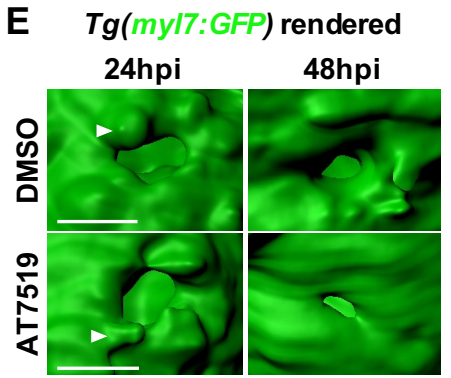
E
Tg(myl7:GFP) rendered
24hpi
48hpi
DMSO
AT7519

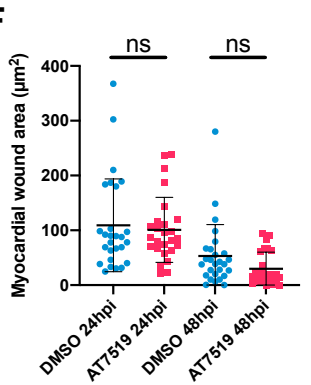
F
Myocardial wound area (μm²)
ns
ns
DMSO 24hpi
AT7519 24hpi
DMSO 48hpi
AT7519 48hpi

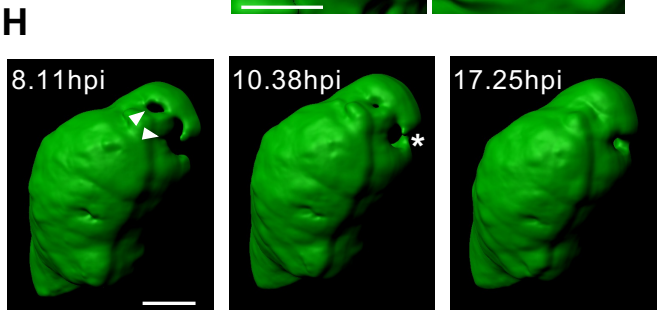
H
8.11hpi
10.38hpi
17.25hpi

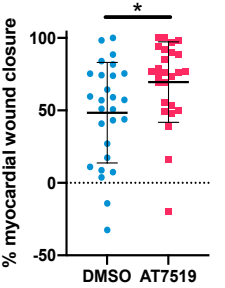
G
% myocardial wound closure
*
DMSO
AT7519

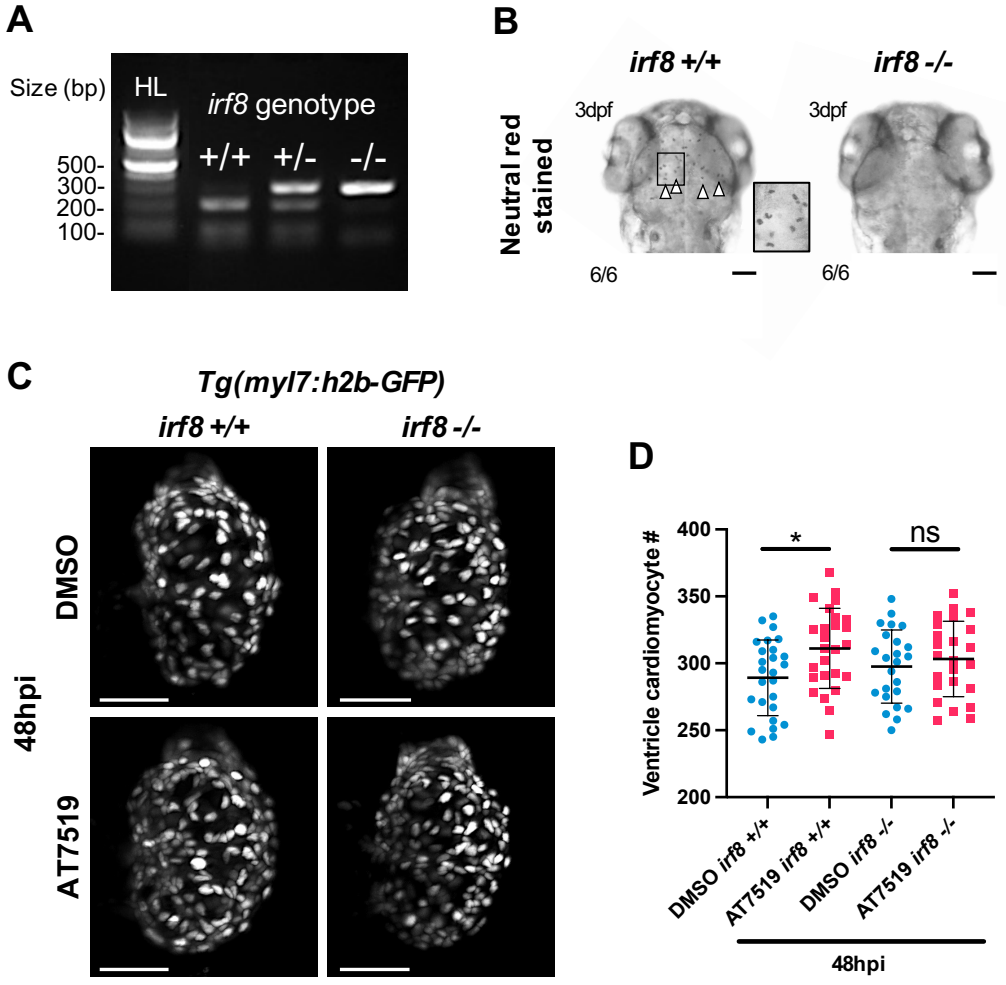
A
Size (bp)
HL
irf8 genotype
+/+
+/-
-/-
500-
300-
200-
100-
B
irf8 +/+
irf8 -/-
Neutral red stained
3dpf
3dpf
6/6
6/6
C
Tg(myl7:h2b-GFP)
irf8 +/+
irf8 -/-
DMSO
AT7519
48hpi
D
Ventricle cardiomyocyte #
400
350
300
250
200
*
ns
DMSO irf8 +/+
AT7519 irf8 +/+
DMSO irf8 -/-
AT7519 irf8 -/-
48hpi